Electronic Supplementary Material (ESI) for Polymer Chemistry.

Supporting information for:

Fluorescent Bowl-shaped Nanoparticles from 'Clicked' Porphyrin-Polymer Conjugates

Derrick A. Roberts,[†,‡] Maxwell J. Crossley,[*,‡] and Sébastien Perrier[*,¶]

Key Centre for Polymers and Colloids, School of Chemistry, The University of Sydney, NSW 2006, Australia, and Department of Chemistry, The University of Warwick, Coventry, CV4 7AL, UK.

E-mail: maxwell.crossley@sydney.edu.au; s.perrier@warwick.ac.uk

[*]To whom correspondence should be addressed
[†]Key Centre for Polymers and Colloids, The University of Sydney, NSW 2006, Australia
[‡]School of Chemistry, The University of Sydney, NSW 2006, Australia
[¶]Department of Chemistry, The University of Warwick, Coventry, CV4 7AL, UK.

Contents

S.1 Experimental Details

S.1.1 Materials

Commercial solvents and reagents were used without further purification unless specified otherwise. Chloroform used for synthesised was stabilised with amylene. 2-(Butylthiocarbonothioylthio)propanoic acid (PABTC) and 2,2′-azobisisobutyronitrile were received from DuluxGroup Australia. (Prop-2-ynyl propanoate)yl butyl trithiocarbonate (PYPBTC) RAFT agent was synthesized by Dr Raphael Barbey (KCPC, The University of Sydney, Australia) using a procedure based on that of Konkolewicz *et al.*[1] The di- and tetraazidoporphyrin starting materials (**DN$_3$PP** and **TN$_3$PP**, respectively) were synthesised according to a previously reported method.[2] Tetrahydrofuran (THF) was distilled from the sodium–benzophenone ketyl under N_2 to remove water and the inhibitor (4-hydroxy-3,5-di-*tert*-butyltoluene).

S.1.2 Instrumentation for Characterization

Microwave syntheses were performed on an A.I. Scientific CEM Discover S-Class synthesis microwave using 5 mL borosilicate sealable microwave tubes. Reaction sequences were programmed using A.I. Scientific Discover software. Flash chromatography was performed using Davisil LC60A 40–63 μm chromatographic silica. Analytical thin layer chromatography (TLC) analyzes were performed on Merck silica gel 60 F_{254} pre-coated sheets. Kugelrohr distillation was carried out using a Büchi GKR-51 glass oven with vacuum supplied by a standard laboratory rotary vacuum pump. Preparative size-exclusion chromatography (SEC) was conducted using a gravity fed column (3 cm internal diameter $\times$ 40 cm) containing Bio-Rad Biobeads® S-X1 cross-linked polystyrene size-exclusion matrix using toluene as the eluent (flow rate 0.5 mL min^{-1}). Melting points were recorded on a Stanford Research Systems OptiMelt System.

Optical absorption spectroscopy was performed on Varian Cary 4000 (900-200 nm) UV-visible spectrophotometer. Solvents were of spectroscopic grade or redistilled according to literature methods.[3] Chloroform was de-acidified prior to use by filtration through a plug of basic alumina

(Brockmann Grade I).

Diffuse Reflectance Infrared Fourier Transform Spectroscopy (DRIFTS) was performed on a Varian 800 Scimitar Series FT-IR spectrometer. Spectra were recorded with a resolution of 4 cm^{-1} for 16 repetitions.

^{1}H NMR and ^{13}C NMR spectra were recorded on Bruker Avance DPX 200 (200 MHz), DPX 300 (300 MHz) and DPX 500 (500 MHz) spectrometers, depending on departmental availability. Deuterated chloroform was de-acidified prior to use by filtration through a plug of basic alumina (Brockmann Grade I), and the TMS peak at 0.00 ppm was used as an internal reference. Signals are recorded in terms of chemical shift (in ppm), relative integral, multiplicity, coupling constants (in Hz) and assignment, in that order. The following abbreviations for multiplicity are used: s, singlet; d, doublet; t, triplet; m, multiplet; br, broad. Recycle delays used for these experiments were five times the T_1 value of the slowest-relaxing proton resonance (usually H_β of the porphyrin moiety or the acetylene proton of the end-functionalised polymer). T_1 values were measured using the inversion-recovery method (standard Bruker program *t1ir1d*), and were typically between 1.8 and 2.8 s for the PPCs and up to 10 s for the acetylene protons. We employ these relaxation delays in order to perform quantitative integration analysis of the polymer end-groups in order to assess end-group fidelity.

Two-dimensional NMR spectra were recorded at 300 K on a Bruker Avance DPX 500 MHz NMR spectrometer, using a BBO two-channel probe that was automatically tuned and matched to the correct operating frequencies for ^{1}H and ^{13}C. Pulse calibration (90°) was routinely performed for ^{1}H experiments (typically $\sim 12.3\,\mu$s at 15.488 W), and T_1 values were estimated by the inversion-recovery method using the standard Bruker pulse program *t1ir1d*. Spectra were processed using Varian Topspin 3 and Mestrenova Lite software. Manual phase correction and automatic baseline correction were applied to all spectra, and the slope and bias values of the peak integrals were adjusted manually to obtain valid integration.

Molecular weight distributions of polymers were measured by analytical Gel Permeation Chromatography (GPC) either on a Shimadzu LC-10AT (hydrophobic polymers) or an Agilent GPC50

(hydrophilic polymers) liquid chromatography system. The Shimadzu system was fitted with a PLgel 5 μm MiniMIX-C (50 × 4.6 mm) guard column and two PLgel 5 μm MIXED-C (300 × 7.5 mm) columns, and equipped with a Shimadzu RID-10A differential refractive index detector (DRI) and a Shimadzu SPD-10A UV-visible absorption detector. Tetrahydrofuran (THF) containing 1,4-hydroquinone (0.04 g L^{-1}) was used as the mobile phase, eluting at 1.0 mL min^{-1} at 40 °C. Analyte samples were dissolved in tetrahydrofuran (THF) spiked with 0.5 vol.% toluene as flow rate marker and filtered (polytetrafluoroethylene, 0.45 μm pore size) prior to injection (100 μL). Chromatograms were calibrated using linear polystyrene standards. Experimental molecular weight (M_n) and dispersity ($Đ$) values of the synthesised polymers were determined by conventional calibration using Cirrus software. The Agilent system was equipped with a Polar Gel-M (50 × 7.5 mm) guard column and two Polar Gel-M (300 × 7.5 mm) columns, using DMF containing 0.1 wt.% LiBr as the eluent, flowing at 1.0 mL min^{-1} at 50 °C. Chromatograms were measured using the integrated RI detector and viscometer. Linear polystyrene standards were used to calibrate the SEC system. Analyte samples were dissolved in DMF spiked with water (0.5 vol.%) as the flow rate marker.

S.1.3 Synthesis of *meso*-5,10,15,20-Tetra(4-azidomethylphenyl)porphyrinatopalladium(II), TN_3PP-Pd

TN_3PP-2H (50 mg, 60 μmol) and palladium(II) acetate (54 mg, 0.24 mmol) were dissolved in a mixture of chloroform (10 mL) and methanol (2 mL), and the solution was stirred at room temperature for 2 h, monitoring the formation of product by TLC. After 5 mins, a bright orange band was observed by TLC (R_f = 0.47; silica; light petroleum/CH_2Cl_2 = 1:1). Once the reaction was complete, the solution was transferred to a separating funnel and the organic layer washed with water (3 × 200 mL), brine (1 × 200 mL), dried over Na_2SO_4, filtered and the solvents removed to afford the crude product. Recrystallisation from $CHCl_3$-MeOH afforded the pure product as a bright orange microcrystalline solid (49 mg, 86 %). IR (DRIFTS, KBr matrix) ν_{max}:3025, 2929, 2100 (N_3), 1353, 1240, 1079, 1013, 857, 799, 716 cm^{-1}. ^{1}H NMR (500 MHz, $CDCl_3$-TMS) 8.80

(8H, s, β-pyrrolic H), 8.19 (8H, d, $J = 7.9$ Hz,phenyl H_o), 7.70 (8H, d, $J = 7.9$ Hz, phenyl H_m), 4.72 (8H, s, CH_2N_3). ^{13}C NMR (125 MHz, $CDCl_3$-TMS) 141.7 (α-pyrrole), 141.5 (phenyl C_{ipso}), 135.1 (phenyl C_{ortho}), 134.4 (phenyl C_{para}), 131.0 (β-pyrrole), 126.6 (phenyl C_{meta}), 121.2 (porphyrin C_{meso}), 54.9 CH_2N_3).

S.1.4 Synthesis of RAFT Polymers

Alkyne-functionalised RAFT polymers were obtained from a pre-synthesized library prepared by members of the Key Centre for Polymers and Colloids, University of Sydney. Table 1 summarizes the RAFT polymers used in this study. The general procedure for synthesising alkyne-functionalised RAFT polymers has been described elsewhere.[4,5]

Table 1: Characterization data for alkyne-RAFT polymers used to prepare the PPCs.

Polymer	$M_{n,theor}$ g mol^{-1}	$M_{n,NMR}$[a] g mol^{-1}	DP_{NMR}	$M_{n,GPC}$ g mol^{-1}	$Đ$ (GPC)	Contributor[b]
PS_{20}	2050	2350	20	2050	1.17	DR
PS_{30}	3850	3400	30	2900	1.13	RC
PS_{40}	4600	4450	40	5150	1.19	DR
PBA_{15}	2050	2200	15	2350	1.15	MD
PtBA_{19}	2700	2700	19	2800	1.24	MD
$PNIPAM_{33}$	3900	4000	33	5900	1.13	DR
$PHEA_{42}$	4600	5150	42	4300	1.24	MD
$PDMA_{15}$	1350	1750	15	1125	1.30	RB

[a] $M_{n,NMR}$ values were determined by quantitative ^{1}H NMR end-group analysis, integrating against the resonance at $\sim$0.9 ppm of the CTA residue (6H for PS, 3H for PBA and PtBA).
[b] Contributors include: Derrick Roberts (DR), Dr Robert Chapman (RC), Dr Maarten Danial (MD) and Dr Raphael Barbey (RB).

RAFT polymerisation of *N*-isopropyl acrylamide (synthesis of PNIPAM$_{33}$)

N-Isopropyl acrylamide (2.0 g, 18 mmol), PYPBTC (148 mg, 0.54 mmol), 2,2′-azobisisobutyronitrile (8.8 mg, 54 μmol) and dioxane (5 mL) were combined in a 21 mL scintillation vial sealed with a rubber septum and the solution solution bubbled with N_2 for 15 min, protected from light. The reaction mixture was heated at 60 °C, monitoring conversion by ^{1}H NMR. After 4 h the reaction mixture was chilled on ice and exposed to air to quench the reaction. The crude yellow product was diluted with minimal THF (∼10 mL) and precipitated by drop-wise addition into hexane/diethyl ether (4:1) stirring at 0 °C. The resulting suspension was filtered and the product obtained as a fine, pale yellow solid. $M_{n,GPC}$ (THF) = 5900 g mol^{-1}, $Đ$ = 1.13. ^{1}H NMR (500 MHz, $CDCl_3$-TMS) (assignments refer to Figure S1) 6.36 (33H, br m, NH), 4.66 (1H, br m, H_g), 4.01 (36H, br m, H_m + H_b [buried] + H_c [buried]), 3.35 (2H, brm, H_h), 2.31–1.12 (108H, br m, H_a + H_d + H_e + H_f + H_i + H_j + H_k), 1.14 (198H, br s, H_l).

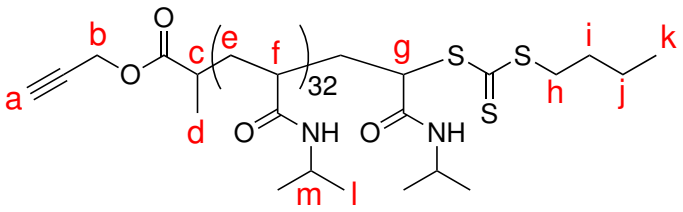

Figure S1: Structure of alkyne-functionalised PNIPAM$_{33}$. Alphabetical labels are referred to for ^{1}H NMR assignment.

S.1.5 Optimisation of CuAAC Coupling Conditions

The conditions for performing CuAAC coupling were initially optimised using alkyne–**PS**$_{30}$ and both **TN**$_3$**PP-Zn** and **DN**$_3$**PP-Zn**. CuAAC coupling was performed using a constant amount of copper(II) sulfate and sodium ascorbate, heating under microwave irradiation (100 °C, 100 W) for up to 30 min in different solvent mixtures.

Initially, an aqueous mixture of THF and pyridine was used to prepare samples of **(PS**$_{30}$**)**$_2$**-Zn** and **(PS**$_{30}$**)**$_4$**-Zn**. After microwave heating, TLC analysis of the crude reaction mixture in chloroform/pyridine (99:1) revealed that the azidoporphyrin starting material had not been completely

consumed. Analysis of the reaction mixture by GPC using DRI and UV-Vis detection (410 nm) revealed a non-uniform mixture of polymeric products with a broad molecular weight distribution, as well as a low molecular weight band corresponding to the unreacted porphyrin starting material.

When performed using DMF as the solvent, CuAAC coupling afforded a much more well-defined product, as can be seen by comparing GPC traces of **$(PS_{30})_2$-Zn** and **$(PS_{30})_4$-Zn** prepared by the THF and DMF methods (Figure S2). In both instances the DMF method produced PPCs with a much narrower molecular weight distribution than the THF method, and also suppressed the formation of high molecular weight by-products. Work-up of the crude porphyrin-polystyrene conjugates involved rotary evaporation, dilution of the reaction mixture with ethyl acetate and passage through alumina to remove any residual copper salts and copper(0) by-products formed during the reaction.[6–8] The eluate was then washed several times with deionised water to remove any remaining DMF (4-5 washes were required) and dried *in vacuo* at 50–60 °C.

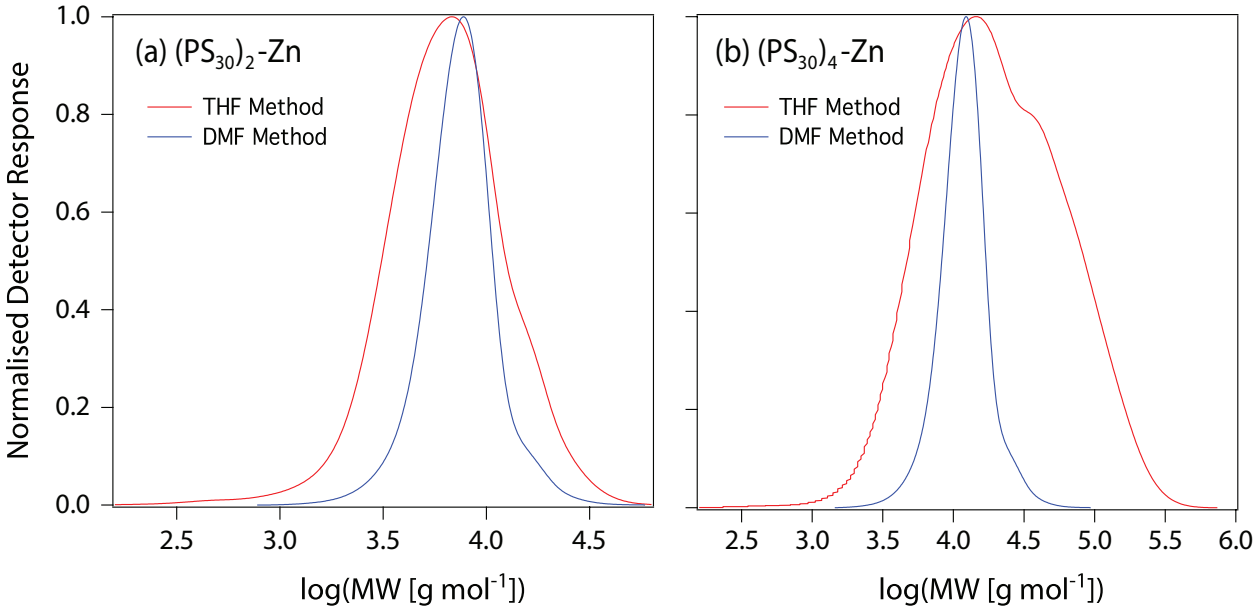

Figure S2: Comparison of analytical GPC traces (THF, 40 °C, 1 mL min^{-1}) of (a) **$(PS_{30})_2$-Zn**; and (b) **$(PS_{30})_4$-Zn**, prepared by the THF and DMF methods under UV-Vis detection at 410 nm. In both cases the DMF method gave conjugates with relatively narrow molecular weight distributions ($1.26 < Đ < 1.30$) and minimal tailing. On the other hand, the THF method gave poorly defined conjugates — most likely a mixture of products with different grafting densities — with significant tailing toward high molecular weight in the 4-arm instance.

The most consistent coupling results were obtained using a 5–10 mol% excess of alkyne polymer with respect to the azide functional groups. Consequently, GPC traces of crude **$(PS_{30})_4$-Zn** and **$(PS_{30})_2$-Zn** under DRI detection were bimodal, with peaks corresponding to the excess **PS_{30}** as well as the target conjugate (Figure S3a). DRI detection is sensitive to any material within the analyte sample that alters the refractive index of the mobile phase; this includes both the porphyrin-polymer conjugates and any uncoupled porphyrin or polymer starting materials. By contrast, UV-Vis detection can be tuned specifically to the peak absorption of porphyrin chromophore at 410 nm (Figure S3b), thus enabling selective detection of porphyrin-containing species (conjugates and azidoporphyrins).[9] Figure S3b shows that the azidoporphyrin was completely consumed in the reaction, and that the porphyrin-polystyrene conjugates eluted as well-defined bands with moderate molecular weight distributions ($Đ$ = 1.21 and 1.38) and no tailing towards low molecular weight.

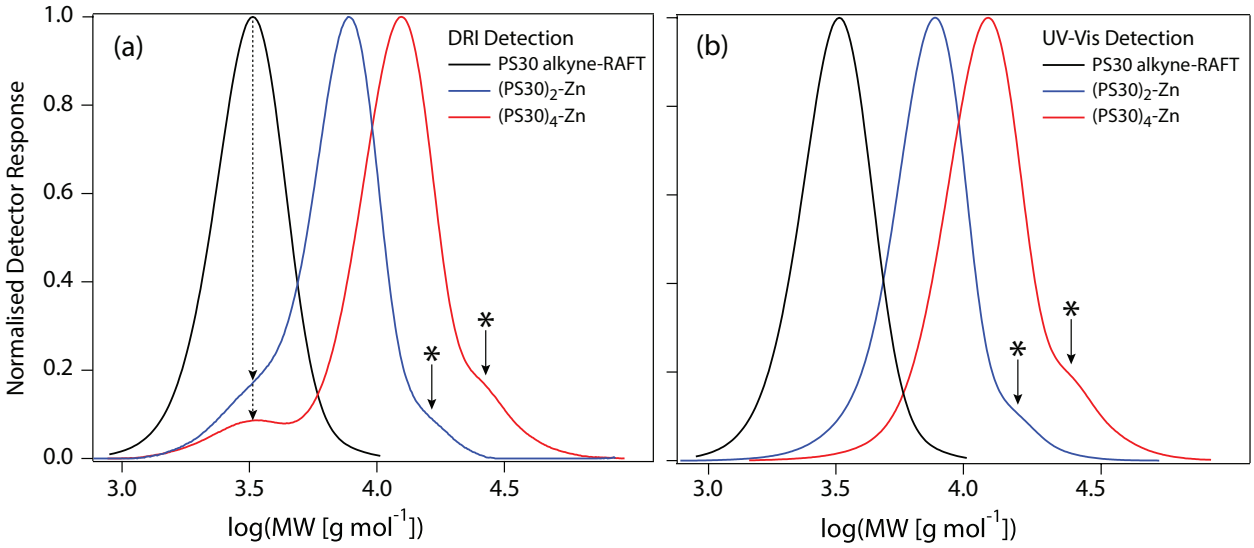

Figure S3: Analytical GPC traces (THF, 40 °C, 1 mL min^{-1}) of alkyne-**PS30**, **$(PS_{30})_2$-Zn** and **$(PS_{30})_4$-Zn** prepared by the DMF method. (a) DRI detection shows low molecular weight shoulders corresponding to the free **(PS_{30})** (b) UV-Vis detection (410 nm for the conjugates; 315 nm for alkyne-PS30) shows that the conjugates possess relatively low dispersities ($Đ$ = 1.21 for **$(PS_{30})_2$-Zn**; $Đ$ = 1.38 for **$(PS_{30})_4$-Zn**). High molecular weight anomalies are marked with asterisks.

We were unable to isolate and characterise the high MW anomalies shown in Figure S3.These high MW shoulders appeared most noticeably in the GPC traces of the four-arm conjugates, and were present both *before and after* fraction on Biobeads SX-1 (Figure S4). The persistent nature of

the high MW anomalies suggests that they might arise from PPC aggregation. Indeed, we observed some evidence of persistent self-assembled oligomers (possibly dimers) at low concentrations for the 4-arm PPCs in our previous study on the coordination-driven self-assembly of hydrophobic PPCs.[2]

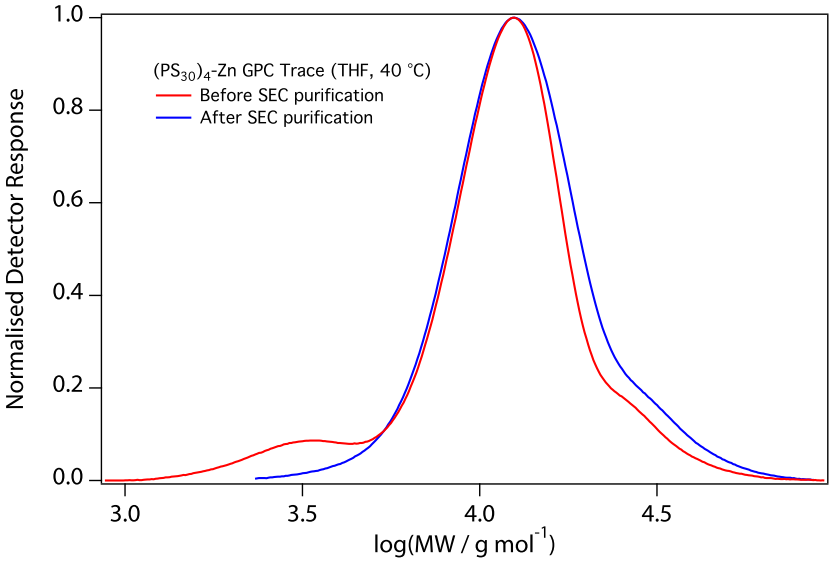

Figure S4: GPC traces of the 4-arm hydrophobic PPCs generally showed a small high MW shoulder, which persisted even after fractionating the crude PPC reaction mixture on Biobeads SX-1. The persistence of this high MW fraction, which resides at approximately twice the number-average molecular weight of the main distribution, suggests that it might form due to dimerisation of the PPCs, possibly through cooperative porphyrinatozinc(II)–triazole coordination. The low MW band in the trace of the crude PPC (red) is due to excess alkyne-polystyrene starting material.

S.1.6 Synthesis of Porphyrin-Polymer Conjugates

Example Procedure: Synthesis of **$(PS_{30})_4$-Zn** is described. Azidoporphyrin **TN_3PP-Zn** (10 mg, 11.1 mmol), alkyne-functionalised RAFT polystyrene (DP = 30, 147 mg, 49.0 mmol), copper(II) sulfate pentahydrate (1.7 mg, 6.7 mmol) and sodium ascorbate (7.7 mg, 39.0 mmol) were weighed into a 10 mL sealable microwave tube. DMF (3 mL) was added, a magnetic stirrer bar added and the vessel sealed. The reaction mixture was sonicated briefly, then heated under microwave irradiation (100 W, 100 °C) for 20 min then allowed to cool. Work-up procedure consisted of passing the crude reaction mixture directly through a short alumina column (Brockmann grade I), then diluting

Table 2: Average molar masses and dispersity values of porphyrin-polymer conjugates before and after preparative SEC.[a]

	GPC data (before prep. SEC)			GPC data (after prep. SEC)			
Conjugate	M_p[b]	M_n[b]	$Đ$	M_p[b]	M_n[b]	$Đ$	$M_{n,theor}$[c]
$(PS_{20})_2$-Zn[d]	5450	3700	1.35	5400	5170	1.18	5350
$(PS_{30})_2$-Zn[d]	7700	6300	1.22	7700	7150	1.19	7450
$(PS_{40})_2$-Zn[d]	12400	8550	1.35	12400	10200	1.25	9500
$(PS_{20})_4$-Zn[d]	8500	4850	2.03	9450	9400	1.30	10340
$(PS_{20})_4$-Pd[d]	10000	3700	2.34	10100	7800	1.70	10380
$(PS_{30})_4$-Zn[d]	12500	9650	1.38	11300	10800	1.26	14500
$(PS_{40})_4$-Zn[d]	19650	15150	1.30	18800	15250	1.25	18700
$(PBA_{15})_4$-Zn[d]	9050	5300	1.52	9800	9200	1.24	9700
$(PtBA_{19})_4$-Zn[d]	12000	8150	1.45	12200	11800	1.20	11750
$(PDMA_{15})_4$-Zn[e]	5500	900	5.57	5500	4200	1.59	7950
$(PNIPAM_{33})_4$-Zn[e]	17400	11600	1.43	17350	14550	1.23	16950
$(PHEA_{42})_4$-Zn[e]	18150	13000	1.57	19850	18400	1.35	11300

[a] Average molar masses and dispersity values were determined by GPC under DRI detection and calibrated against linear polystyrene narrow standards.
[b] Molar masses are given in units of $g\,mol^{-1}$.
[c] $M_{n,theor}$ was calculated from the average degree of polymerisation of the grafted polymer chains (determined by ^1H NMR) and the molar masses of the porphyrin, CTA and repeat unit.
[d] GPC eluent: THF, flow rate $1\,mL\,min^{-1}$, 40 °C with toluene as flow rate marker.
[e] GPC eluent: DMF, flow rate $0.7\,mL\,min^{-1}$, 50 °C with water as flow rate marker.

with ethyl acetate (ca. 20 mL) and washing the organic phase with deionised water (5×50 mL) to remove the DMF. The organic layer was dried over Na_2SO_4, filtered and the solvents removed on a rotary evaporator. The resulting amorphous purple solid was dissolved in minimal CH_2Cl_2 and precipitated by dropwise addition into methanol at $-78\,^{\circ}C$ to afford the purified polymer as a pale purple powder. For two-arm conjugates, the amount of polymer, catalyst and reducing agent was halved, but reaction volume remained constant.

Characterization Data

Characterisation data for hydrophobic PPCs have been reported in previous work.[2] Spectroscopic data for **(PHEA$_{42}$)$_4$-Zn** and **(PNIPAM$_{33}$)$_4$-Zn** are not provided since incomplete functionalisation of the porphyrin core yielded mixtures of partially-coupled products. The relevant spectra are discussed in Section S.6.

(PDMA$_{15}$)$_4$-Zn: $M_{n,GPC}$ (DMF) = 4190 g mol^{-1}, $Đ = 1.59$. ^{1}H NMR (500 MHz, $CDCl_3$-TMS + 2% d_5-pyridine) 8.80 (8H, s, β-pyrrolic H), 8.17 (8H, d, $J = 7.5$ Hz, phenyl H$_o$), 7.93 (4H, br m, triazole Ar-H), 7.63 (8H, br m, H$_m$), 5.91 (8H, br s, triazole-H$_{N\alpha}$), 5.34 (8H, br m, triazole-H$_{C\alpha}$), 5.21 (4H, m, –C*H*–SCS$_2$), 3.36 (8H, t, $J = 7.4$ Hz, –SC*H*$_2$CH$_2$–), 2.56–1.18 (196H, br m, backbone –CHCH$_2$–, CTA-β,γ–CH$_2$), 2.92 (360H, br s, –N(CH$_3$)$_2$), 1.16 (12H, t, $J = 7.4$ Hz, CTA –O(C=O)CHC*H*$_3$) 0.92 (12H, t, $J = 7.4$ Hz, CTA –SCS$_2$–Bu–CH$_3$).

S.2 Calculation of theoretical number-average molar mass

The theoretical number-average molar mass, $M_{n,theor}$, of each PPC was calculated using the following equation:

$$M_{n,theor} = MW_{porphyrin} + x(MW_{monomer} \times DP) + MW_{CTA} \quad (1)$$

Where x is the number of polymer arms (2 or 4) attached to the porphyrin core, DP is the number-average degree of polymerization of the grafted polymer chains (determined by ^{1}H NMR end-

group analysis of the alkyne-polymer precursor), and MW_{CTA} is the molar mass of the RAFT CTA.

S.3 Calculation of CuAAC reaction efficiency

The reaction efficiency of the CuAAC coupling reaction was estimated the ^{1}H NMR integrals of H_{Tz}, $H_{N\alpha}$ and $H_{C\alpha}$ (see Figure S5 for proton assignments) according to the following equation:

$$X = \frac{I_{NMR}}{I_{theor.}} \times 100 \tag{2}$$

Where X is reaction conversion (expressed as a percentage), I_{NMR} is the integral of a given resonance in the ^{1}H NMR spectrum, and I_{theor} is the theoretical integral of the resonance at 100% conversion. Total estimated conversion (X_{ave}) is given by averaging the individual conversions (X) calculated from the resonances of $H_{N\alpha}$, $H_{C\alpha}$ protons and H_{Tz} (see Table 1, main text). Integrals were calibrated to the porphyrin H_β resonance (8H). The entire β-pyrrolic region was integrated in order to account for all porphyrin-containing species in the sample, i.e., porphyrin starting materials, and both partially and completely functionalized conjugates. Since H_{Tz}, $H_{N\alpha}$ and $H_{C\alpha}$ are unique to the fully- and partially-coupled products, the integrals of these resonances provide a good indication of the reaction conversion.

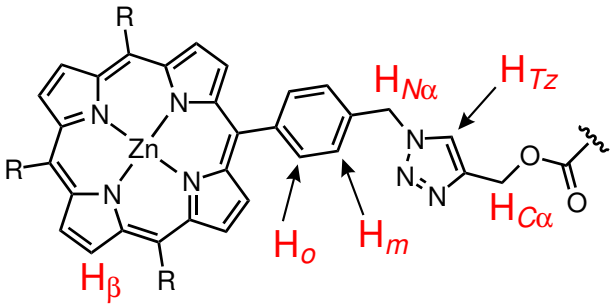

Figure S5: Labelled chemical structure of a generic triazole-appended porphyrin, describing the proton assignments relevant to calculating reaction efficiency.

S.4 Raw GPC data for PPCs

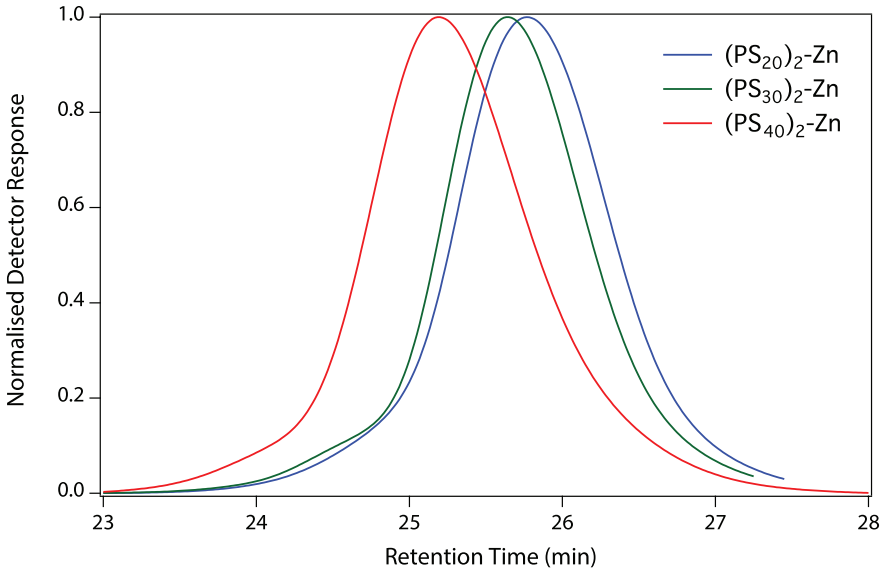

Figure S6: GPC traces (THF) of **(PBA$_{15}$)$_4$-Zn** and **(P*t*BA$_{19}$)$_4$-Zn**.

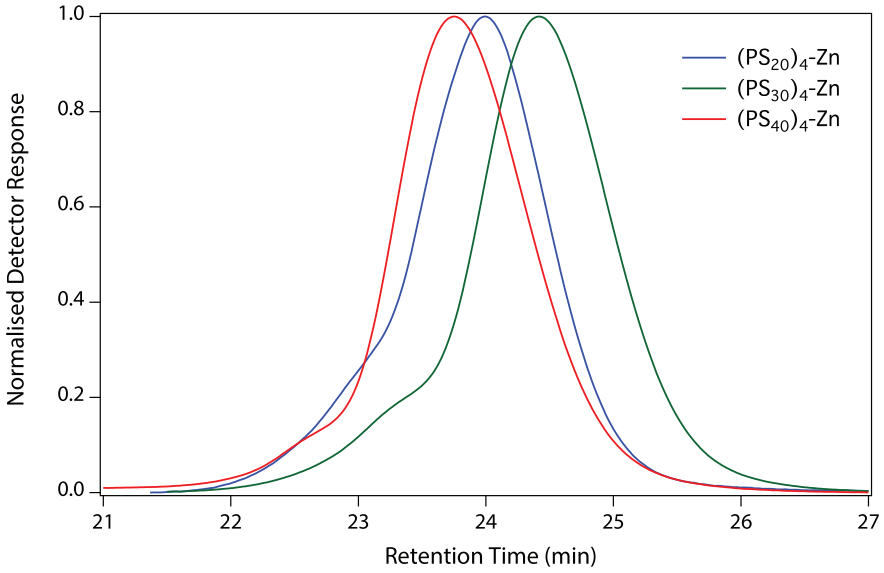

Figure S7: GPC traces (DMF) of hydrophilic porphyrin-polymer conjugates.

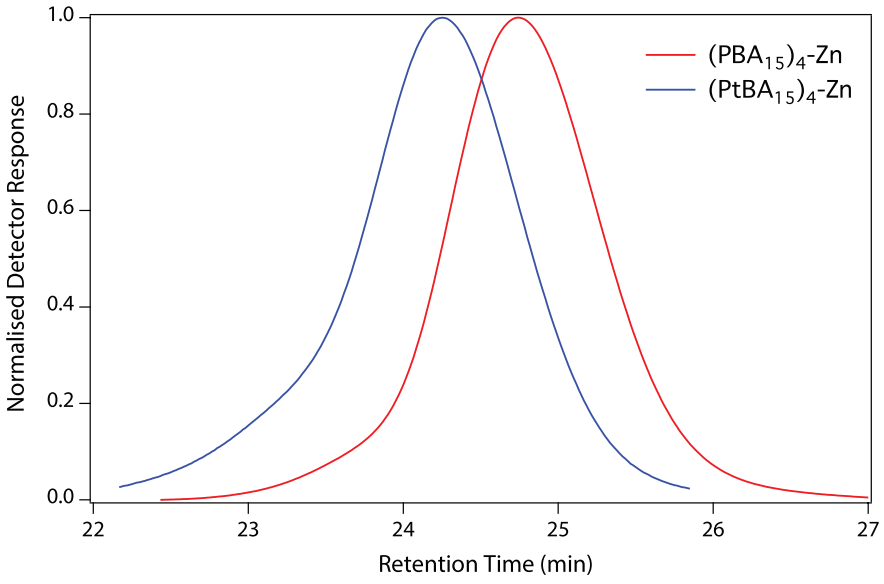

Figure S8: GPC traces (THF) of **$(PBA_{15})_4$-Zn** and **$(PtBA_{19})_4$-Zn**.

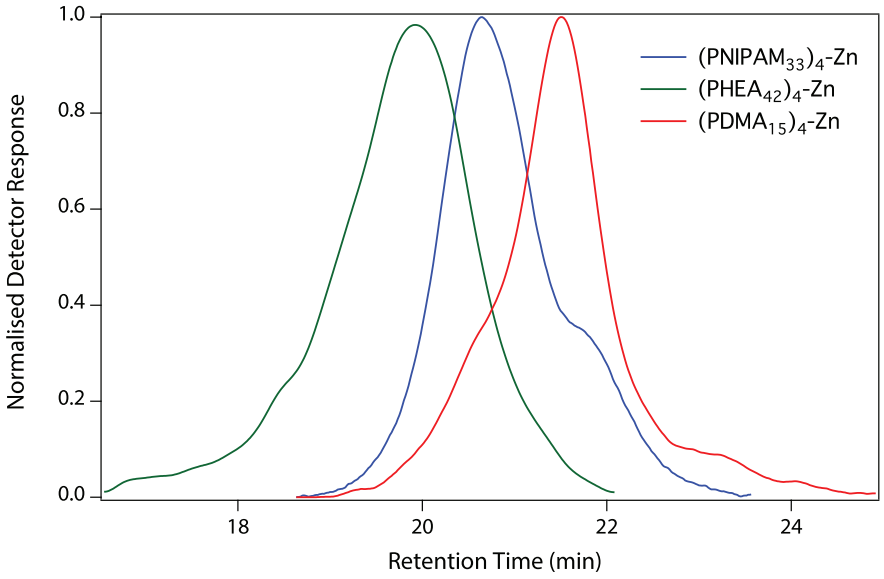

Figure S9: GPC traces (DMF) of hydrophilic porphyrin-polymer conjugates.

S.5 Evidence for Thermal Huisgen Cycloaddition Pathway in Porphyrin–Polymer Coupling

S.5.1 Rationalisation of unusual splitting in ^{1}H NMR spectra of hydrophobic PPCs

In our previous work on hydrophobic PPCs,[2] unusual splitting of the $H_{N\alpha}$, $H_{C\alpha}$ and H_{Tz} resonances was observed in their ^{1}H NMR spectra. This splitting was attributed to a combination of diastereotopic induction from the chiral centre introduced by the polymer repeat units and partial formation of the 1,5-triazole regioisomer due to the non-catalysed thermal azide-alkyne cycloaddition pathway.[10,11]

Chapman *et al.* have also observed splitting of the analogous $H_{N\alpha}$ and $H_{C\alpha}$ protons in the ^{1}H NMR spectra of cyclic peptide–polymer conjugates.[4,5] The authors attributed splitting to restricted rotation of the C–C bonds either side of the triazole ring, arising from the steric bulk and low diffusivity of the grafted polymer chains. Restricted rotation causes protons $H_{N\alpha}$ and $H_{C\alpha}$ to become diastereotopic, resulting in geminal splitting of these resonances into doublets-of-doublets with coupling constants of 12–13 Hz and 26–30 Hz. In the ^{1}H NMR spectra of the porphyrin-polymer conjugates, however, splitting of $H_{N\alpha}$ and $H_{C\alpha}$was not symmetric. Thus, while diastereotopic induction is likely a minor factor in this sytem, it is clearly not the sole reason for the observed splitting. Furthermore, hindered rotation does not explain the splitting observed for H_{Tz}, since it does not have a geminal proton to which it could couple.

To test the hindered rotation hypothesis, the ^{1}H NMR spectrum of **(PS$_{30}$)$_4$-Zn** was recorded at different temperatures from 300–330 K (Figure S10). If restricted rotation of the C–C bonds either side of the triazole ring contributes to splitting of the $H_{N\alpha}$, $H_{C\alpha}$ and H_{Tz} resonances, then increasing temperature should accelerate the rate of single bond rotation and thus collapse the multiplets into singlets. As Figure S10 clearly shows, increasing temperature had no observable effect on the splitting of $H_{N\alpha}$ and $H_{C\alpha}$. Interestingly, splitting of H_{Tz} appears to be temperature-dependent, changing from a broad triplet at 300 K to a broad doublet at 330 K. However, the partial ^{1}H–^{13}C HSQC spectrum in Figure S11 reveals that the broad resonance assigned to H_{Tz} overlaps

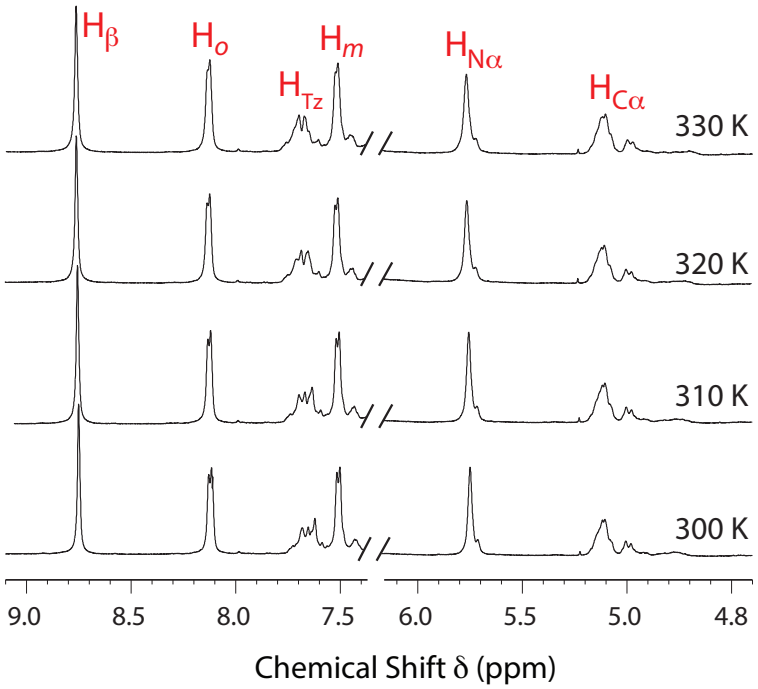

Figure S10: Partial ^{1}H NMR spectra of **(PS$_{30}$)$_4$-Zn** in CDCl$_3$/d_5-pyridine (98:2, *v*/*v*) at 300–330 K. Splitting patterns of the H$_{N\alpha}$ and H$_{C\alpha}$ resonances do not change noticeably as a function of temperature, suggesting that the observed splitting is not caused by restricted rotation. However, H$_{Tz}$ changes from a broad triplet at 300 K to a broad doublet at 330 K.

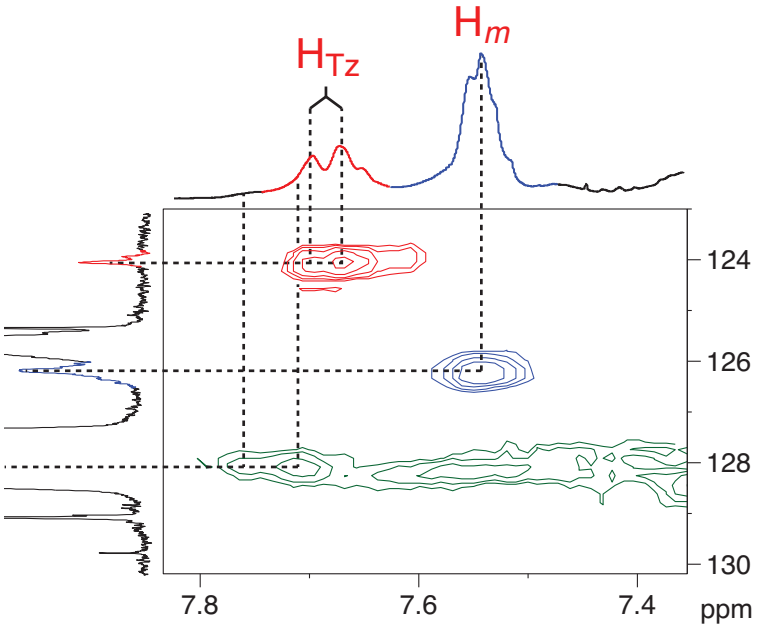

Figure S11: Partial ^{1}H–^{13}C HSQC spectrum (500/125 MHz, 300 K) of **(PS$_{30}$)$_4$-Zn** in CDCl$_3$/d_5-pyridine (98:2, *v*/*v*). The broad multiplet at 7.7 ppm is comprised of two overlapping aromatic proton resonances: H$_{Tz}$ (red) and an unassigned proton environment (green), which has a broad ^{13}C correlation at ∼128 ppm. ^{13}C spectrum has been cropped to highlight the low-intensity resonance at 124 ppm.

with another aromatic proton resonance; therefore, the apparent temperature dependence of the splitting of H_{Tz} is most likely due to independent shifting of these overlapping proton resonances. Nevertheless, the appearance of H_{Tz} as a broad doublet in Figure S11, rather than a singlet, still suggests the presence of at least two different triazole environments.

S.5.2 Thermal Huisgen control experiment

PPC coupling was performed without copper(II) sulfate and sodium ascorbate to test the hypothesis that the thermal Huisgen reaction can occur alongside CuAAC coupling. **TN_3PP-Zn** and alkyne-(**PS_{20}**) were reacted together in DMF at 100 °C, and GPC was performed on aliquots of the reaction mixture after 25, 50 and 75 min of microwave dielectric heating (Figure S12). The chromatograms, collected using UV detection at 410 nm to detect only porphyrin-containing species, clearly show formation of a higher molecular weight species (M_n = 2500 g mol^{-1}) consistent with mono-functionalised **TN_3PP-Zn** after only 25 min of heating. ^{1}H NMR analysis of the reaction mixture revealed triazole peaks consistent with the resonances observed in spectra of PPCs prepared by CuAAC coupling, alongside characteristic peaks of **TN_3PP-Zn** (Figure S13) in an approximately 30:70 ratio when integrated against the H_β peak cluster of the porphyrin species in the ensemble. The ^{1}H NMR spectrum of the reaction mixture also clearly reveals that the peak profile of $H_{C\alpha}$ is split into two approximately even humps, which represent equal formation of the 1,4- and 1,5-triazole isomers under thermal conditions. Additional heating of the reaction mixture increased the production of the higher molecular weight compound, confirming the presence of free (unreacted) alkyne and azide functional groups. Thus, it appears that the thermal Huisgen cycloaddition can indeed occur on the reaction timescales used to prepare the PPCs, consistent with the explanation described in our previous work.

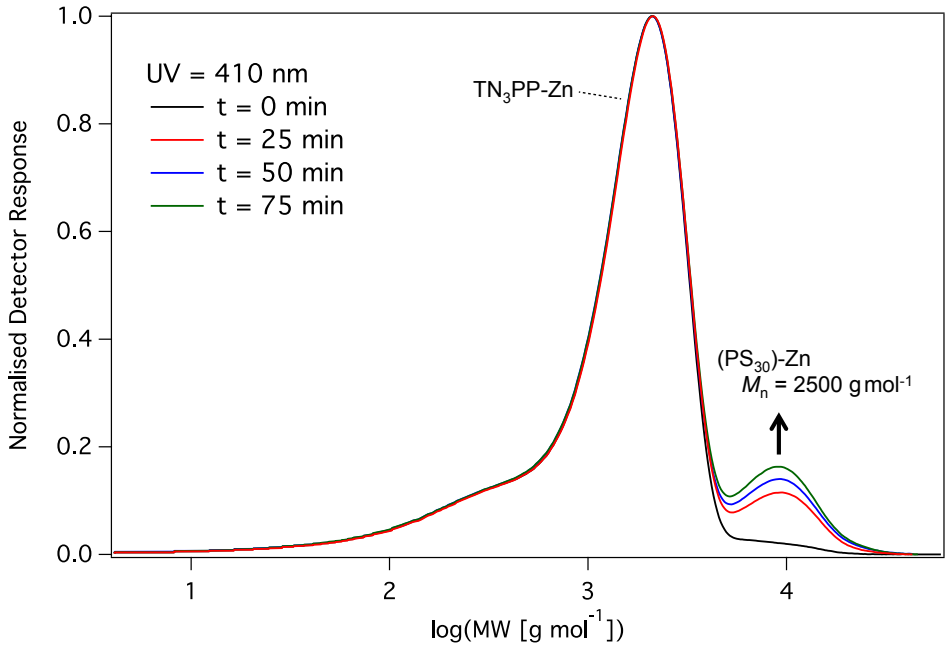

Figure S12: GPC traces of thermal Huisgen control experiment. Chromatograms were collected under UV detection at 410 nm, monitoring the molecular weight distribution of all species bearing a porphyrin chromophore.

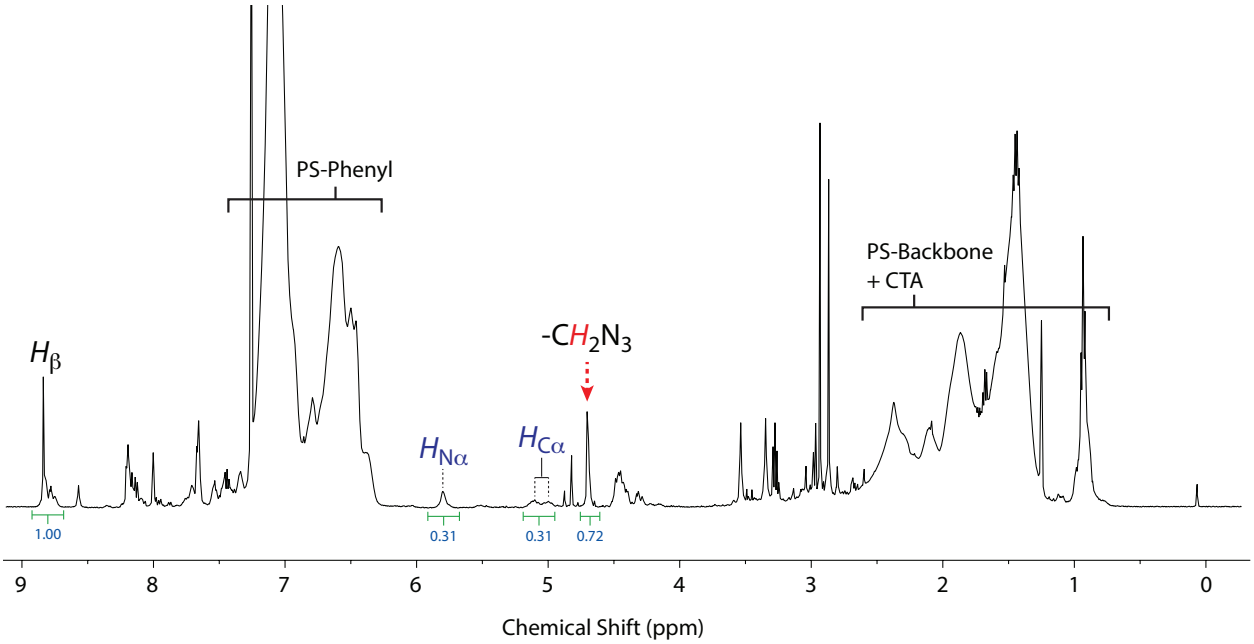

Figure S13: ^{1}H NMR spectrum (500 MHz, 300 K) of the thermal Huisgen test reaction mixture, recorded in $CDCl_3/d_5$-pyridine (98:2, *v*/*v*). The H_β peak cluster is assumed to represent all porphyrin-containing species in the ensemble; thus, integrals of the α-triazole and α-azide methylene resonances represent the starting material and product distributions of the reaction mixture.

S.6 ^{1}H NMR spectra of hydrophilic PPCs

^{1}H NMR spectra of the hydrophilic conjugates (PDMA, PNIPAM and PHEA arms) were partially assigned according to the assignments of related PPCs reported in previous work.[2] As mentioned in the main body of this paper, CuAAC coupling using hydrophilic arms suffered from reduced efficiency compared to their hydrophobic counterparts. Consequently, the following NMR spectra represent mixtures of partially-functionalised products, with the exception of PDMA, which underwent CuAAC coupling without difficulty.

^{1}H NMR spectra of **(PDMA$_{15}$)$_4$-Zn** is free from any porphyrin starting materials and resonances of the porphyrin and phenyl groups (A–C) are reasonably well-defined, suggesting complete functionalisation of the azidoporphyrin. The broadness of $H_{N\alpha}$ (D) and $H_{C\alpha}$ (F) are consistent with the lineshapes observed for the hydrophobic porphyrin-polymer conjugates discussed in the previous section. While $H_{N\alpha}$ does not clearly split into multiple resonances, its broadness and asymmetry still suggests multiple chemical environments. H_{Tz} (E) was not clearly visible, appearing as a broad set of multiplets that could be not assigned to any particular proton environment.

In the ^{1}H NMR spectra of **(PNIPAM$_{33}$)$_4$-Zn** (Figure S15) and **(PHEA$_{42}$)$_4$-Zn** (Figure S16) resonances of the porphyrin and phenyl groups (A–C) are particularly broad and integrals of $H_{N\alpha}$ (D) and $H_{C\alpha}$ (F) are approximately half of their expected values, indicating incomplete conversion of the azidoporphyrin. In Figure S15, the presence of the -CH_2N$_3$ resonance of **TN$_3$PP**-Zn at 4.76 ppm confirms that the azidoporphyrin starting material was not completely consumed during the reaction. Possible explanations for the reduced coupling efficiencies are discussed in the main body of this paper.

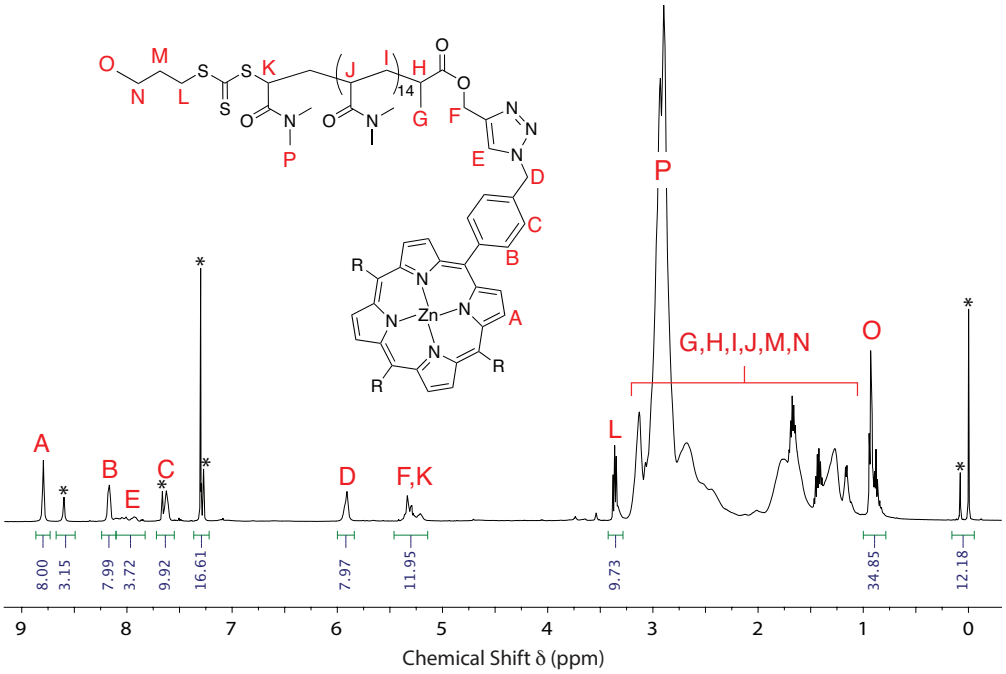

Figure S14: Assigned ^{1}H NMR spectrum (500 MHz, 300 K) of **(PDMA$_{15}$)$_4$-Zn** in CDCl$_3$/d_5-pyridine (98:2, *v*/*v*). Proton assignments: A = H$_\beta$, B = H$_o$, C = H$_m$, D = H$_{N\alpha}$, E = H$_{Tz}$, F = H$_{C\alpha}$. Asterisks denote NMR solvent peaks.

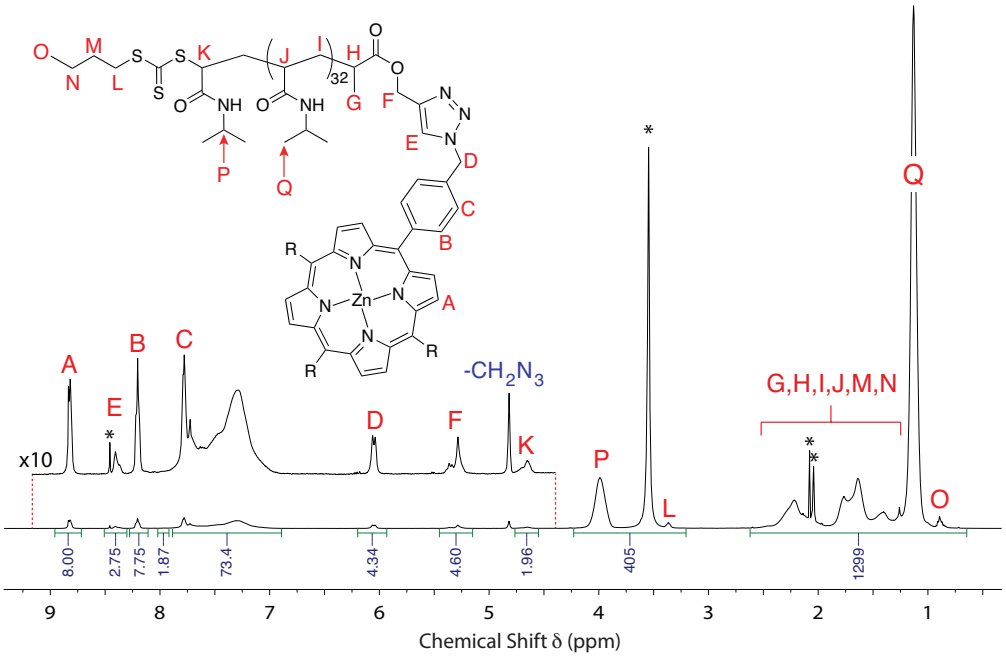

Figure S15: Assigned ^{1}H NMR spectrum (500 MHz, 300 K) of **(PNIPAM$_{33}$)$_4$-Zn** in d_6-acetone containing 2% (*vv*) d_5-pyridine. Proton assignments: A = H$_\beta$, B = H$_o$, C = H$_m$, D = H$_{N\alpha}$, E = H$_{Tz}$, F = H$_{C\alpha}$. Asterisks denote NMR solvent peaks.

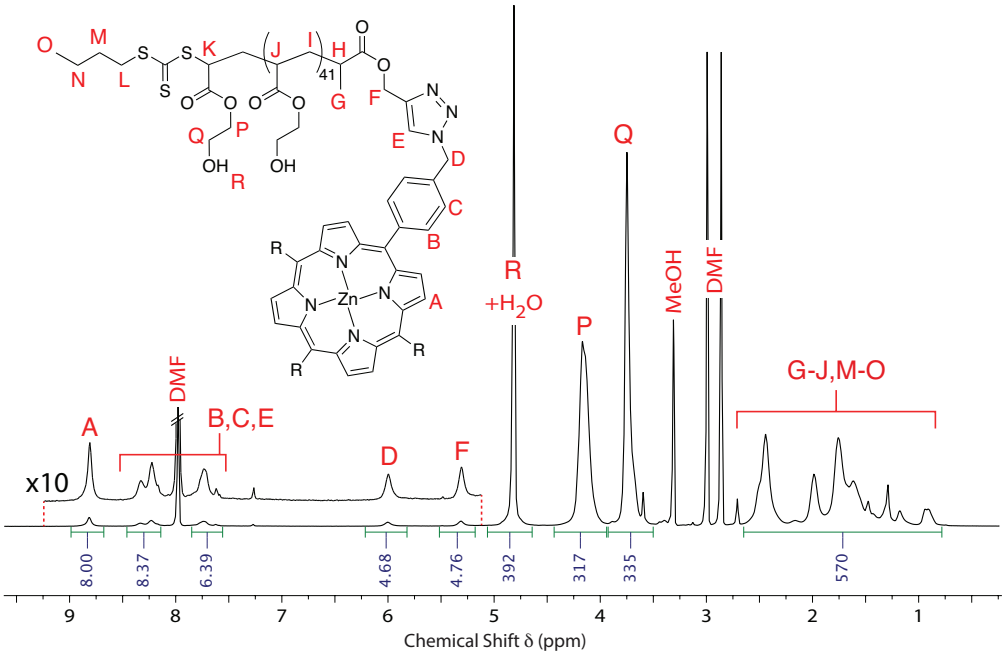

Figure S16: Assigned ^{1}H NMR spectrum (500 MHz, 300 K) of (**PHEA**$_{42}$)$_4$**-Zn** in CD_3OD. Proton assignments: A = H_β, B = H_o, C = H_m, D = $H_{N\alpha}$, E = H_{Tz}, F = $H_{C\alpha}$. Residual solvents are labelled on diagram. Note that the -CH_2N$_3$ resonance of **TN$_3$PP**-Zn is overlapping with resonance *R* of the polymer backbone.

S.7 Post-conjugation Modification Reactions

S.7.1 Re-metallation with Tin(IV)

Since tin(IV) porphyrins are both synthetically and photophysically interesting compounds,[12–25] it is useful to demonstrate the preparation of a tin(IV)-metallated porphyrin-polymer conjugate. **$(PS_{30})_4$-2H** was converted to its dichlorotin(IV) chelate using a modification of the method reported by Crossley and Thordarson.[26] **$(PS_{30})_4$-2H** and tin(II) chloride were heated under microwave irradiation (150 W) in DMF at 150 °C for 30 min. The optical absorption spectrum of the reaction mixture showed complete loss of the freebase absorption bands and appearance of a characteristically red-shifted ($\Delta\lambda = 10$ nm) Soret band and two Q-bands, thus signifying successful formation of **$(PS_{30})_4$-$SnCl_2$** (Figure S17). Peak wavelengths of the major absorption bands and the $\varepsilon(Q_\beta)/\varepsilon(Q_\alpha)$ ratio of 1.53 of the newly-formed dichlorotin(IV) porphyrin-polymer conjugate were nearly identical to values reported in the literature for dichloro(5,10,15,20-tetraphenylporphyrinato)tin(IV).[12]

A typical tin(IV) metallation procedure requires heating of the reaction mixture for 2–4 h.[26,27] The procedure presented here, however, only requires a comparatively brief heating period to achieve the same result. Arnold and Blok recommend that the reaction time for tin(IV) metallation is minimised in order to prevent reduction of the porphyrin to its corresponding chlorin.[12] Chlorin impurities can be identified by a characteristic absorption band at 625 nm. We note the presence of such a band in the optical absorption spectrum of **$(PS_{30})_4$-$SnCl_2$** (Figure S17, labelled '*c*'); however its low intensity suggests that only a small amount of the chlorin by-product was produced.

A pungent thiol-like odour was noted during the work-up of the reaction mixture, suggesting possible damage to the trithiocarbonate group of the CTA residue. A decrease in the trithiocarbonate absorption band intensity (312 nm) following tin(IV) metallation (Figure S17) confirmed degradation. Since tin(IV) metallation involves a tin(II)-to-tin(IV) oxidation step, it is possible that the trithiocarbonate group is reduced under these conditions. The ^{1}H NMR spectrum of **$(PS_{30})_4$-$SnCl_2$**

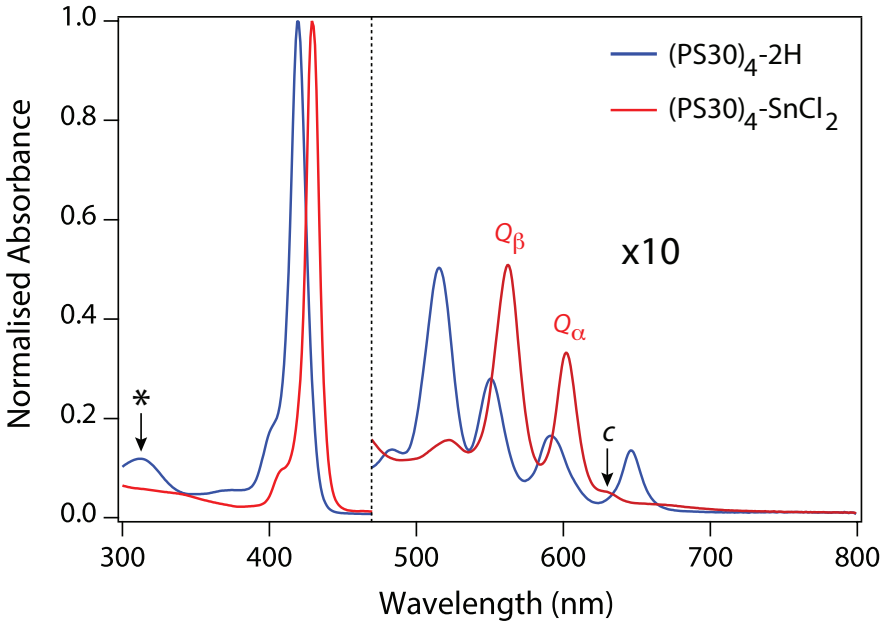

Figure S17: Optical absorption spectra of $(\mathbf{PS}_{30})_4$**-2H** and $(\mathbf{PS}_{30})_4$**-SnCl**$_2$ in $CHCl_3$. $(\mathbf{PS}_{30})_4$**-2H** displays four Q-bands characteristic of a freebase porphyrin, whereas $(\mathbf{PS}_{30})_4$**-SnCl**$_2$ displays three Q-bands and a slightly red-shifted (10 nm) Soret band, which is typical of dichlorotin(IV) porphyrins.[12,26] The trithiocarbonate absorption band at 312 nm is highlighted with an asterisk. A possible chlorin impurity band at 625 nm is labelled '*c*'.

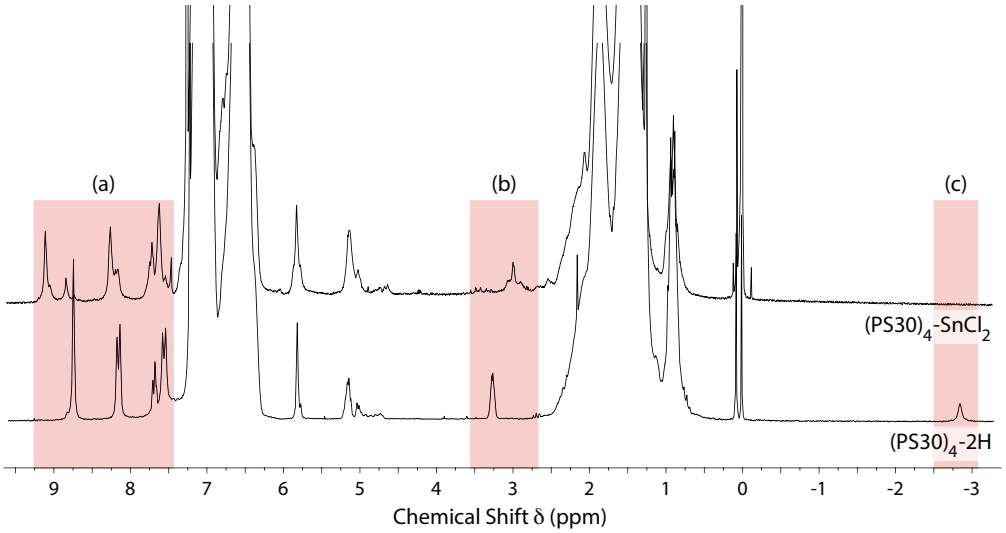

Figure S18: ^{1}H NMR spectra of $(\mathbf{PS}_{30})_4$**-Zn** and $(\mathbf{PS}_{30})_4$**-SnCl**$_2$ ($CDCl_3$, 500 MHz, 300 K). Resonances of the polymer repeat units and backbone have been cropped for clarity. (a) Porphyrin-phenyl-triazole aromatic resonances shift downfield and become broadened multiplets, indicating the presence of degradation products. (b) The SCS_2-α–CH_2 butyl resonance is shifted upfield in the metallated conjugate and its lineshape is severely distorted, suggesting damage to the trithiocarbonate group. (c) Loss of inner NH resonance indicates that the porphyrin was successfully metallated.

further highlights the damage that the conjugate endured as a result of tin(IV) metallation (Figure S18): resonances of the porphyrin-phenyl-triazole spin systems are significantly broader and less-defined than those of the freebase precursor (Figure S18, region [a]). The butyl-α–CH_2 resonance of the CTA residue has also disappeared (Figure S18, region [b]), which is consistent with the decrease in the UV absorption band of the trithiocarbonate group (Figure S17).

Apparent degradation of the tin(IV) porphyrin-polymer conjugate did not significantly affect its peak molar mass, but resulted in a marked increase in dispersity from $Đ$ = 1.26 for **(PS$_{30}$)$_4$-Zn** to $Đ$ = 1.53 for **(PS$_{30}$)$_4$-SnCl$_2$**. However, it is clear from Figure S19 that the molecular weight distribution of the conjugate is still predominantly monomodal and does not show any tailing towards low molecular weights, therefore indicating that the polymer arms were not cleaved from the porphyrin core during metallation.

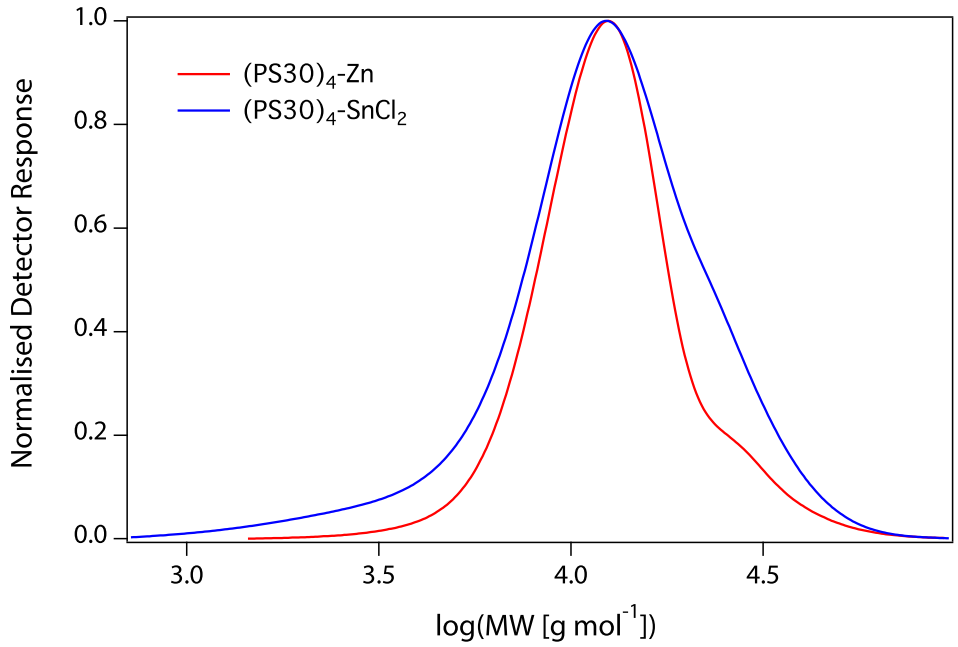

Figure S19: Comparison of the analytical GPC traces (DRI detection) of **(PS$_{30}$)$_4$-Zn** and **(PS$_{30}$)$_4$-SnCl$_2$**. Acidic demetallation and subsequent re-metallation with tin(IV) did not affect M_p of the conjugate, but did result in an increase in dispersity. The absence of low molecular weight bands suggests that the polymer arms were not cleaved from the porphyrin core. Both conjugates show tailing towards high molecular weight, which is attributed to star-star aggregation.

S.8 DLS characterisation of PPC nanoparticles

Dynamic light scattering (DLS) was performed on PPC nanoparticle suspensions (Figure S20) using a Brookhaven BI-200SM goniometer and laser light scattering system operating at 633 nm. The scattering detector was fixed at 90° to the incident laser beam. For suspensions containing THF/water mixtures, refractive indices and viscosities were determined by interpolating published physical data for such mixtures (Figures S21).[28]

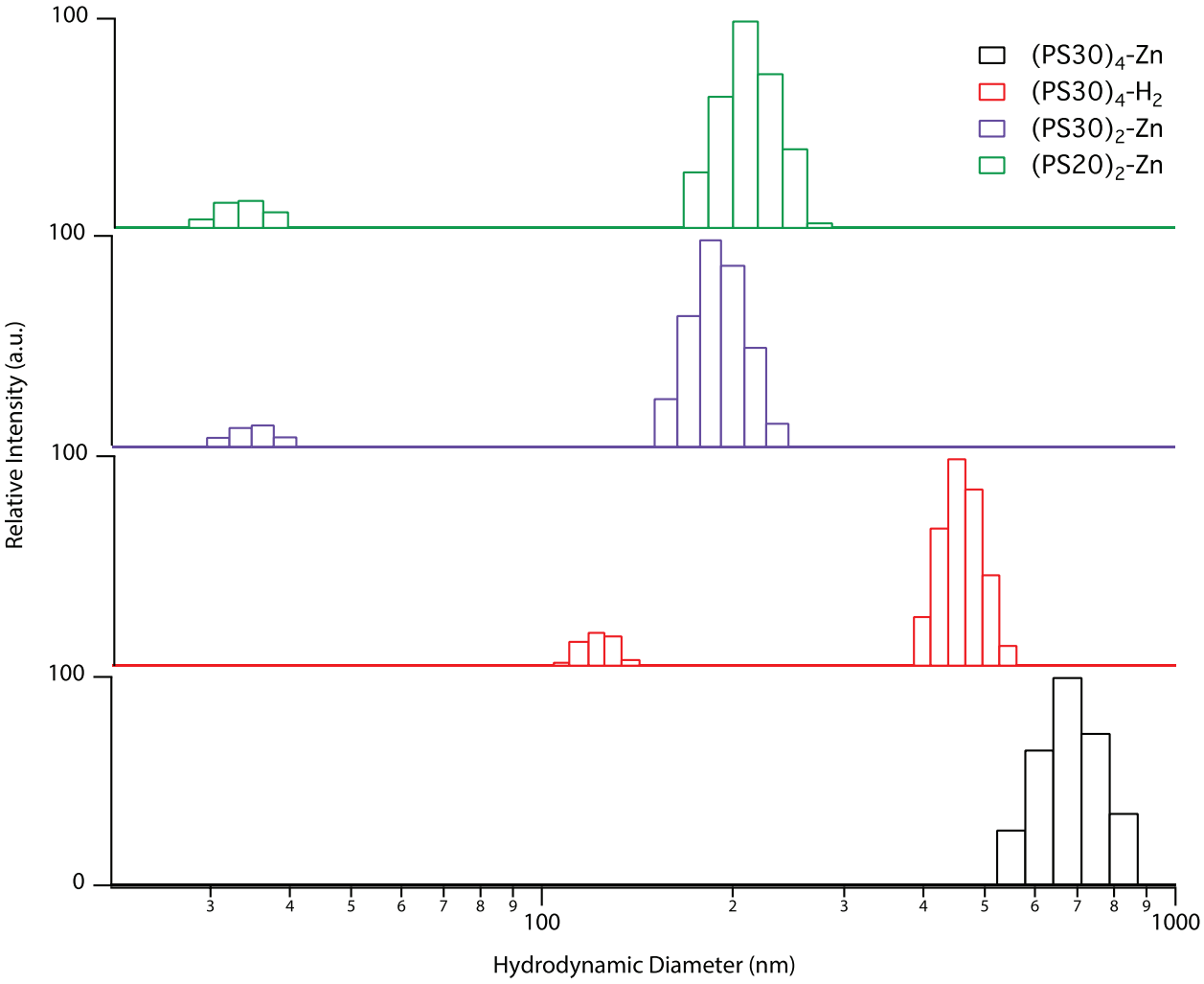

Figure S20: Dynamic light scattering data for nanoparticle suspensions prepared from PPCs. Suspensions contain THF/water mixtures, for which the refractive indices and viscosities were determined by interpolating published data (see Figure S21).

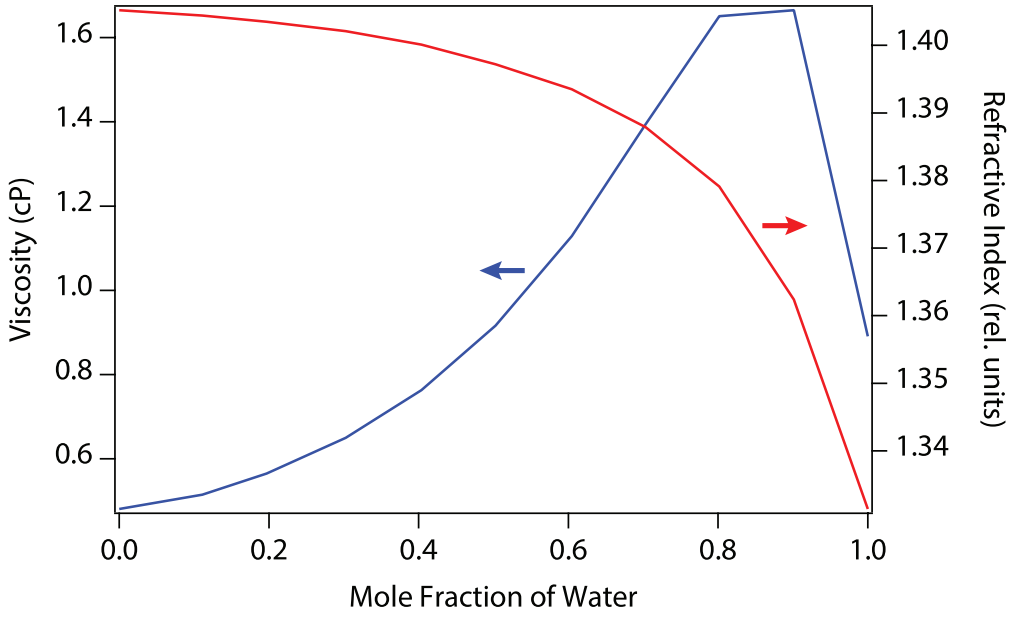

Figure S21: Viscosity and refractive index values of THF/water mixtures used for DLS measurements.[28]

S.9 TEM images of PPC nanoparticles

Transmission electron microscopy (TEM) was carried out on a Philips CM120 Biofilter microscope using carbon-coated copper grids (100-200 mesh). Nanoparticle suspensions were drop-cast onto the grids and allowed to dry in air prior to analysis. Grids were analysed without staining. Cryomicrotomy was performed by mixing aqueous nanoparticle suspensions with sucrose solution (2.3 M), followed by sectioning at −120 °C. 70–90 nm sections were collected on Lacey Formvar grids and any remaining sucrose was removed by gentle washing with water. Cryomicrotomy was undertaken by Dr Delfine Cheng of the Australian Microscopy and Microanalysis Facility at the University of Sydney, Australia.

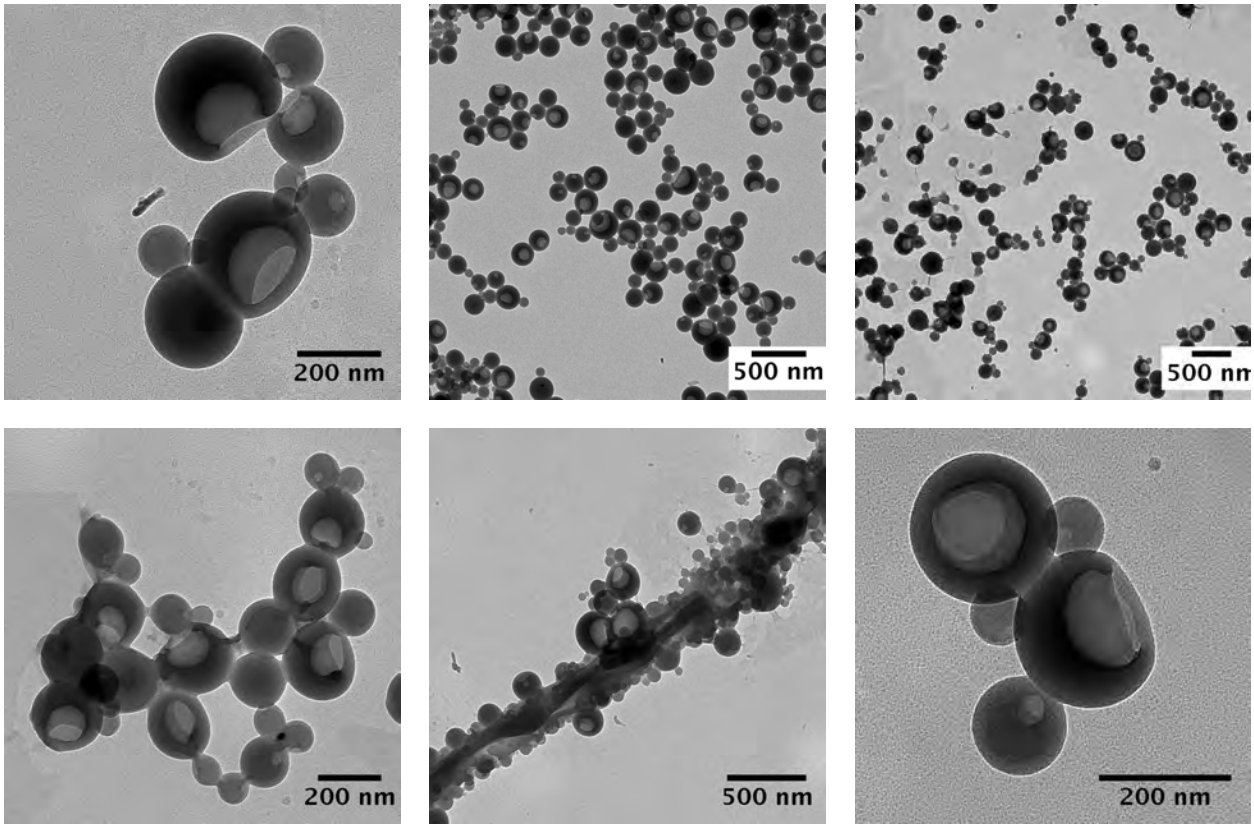

Figure S22: TEM images of **$(PS_{20})_2$-Zn** nanoparticles. Dimpled nanoparticle formation is prominent through the sample. Images were recorded from two separate samples across three grid areas each.

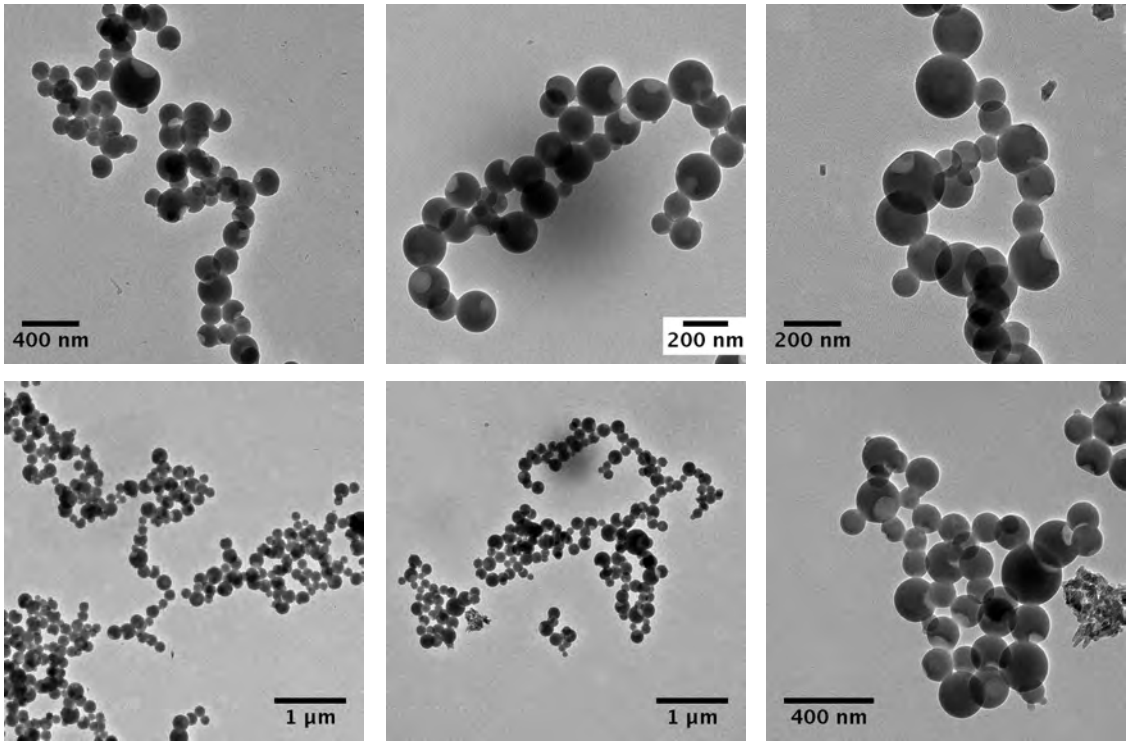

Figure S23: TEM images of **$(PS_{20})_4$-Zn** nanoparticles.

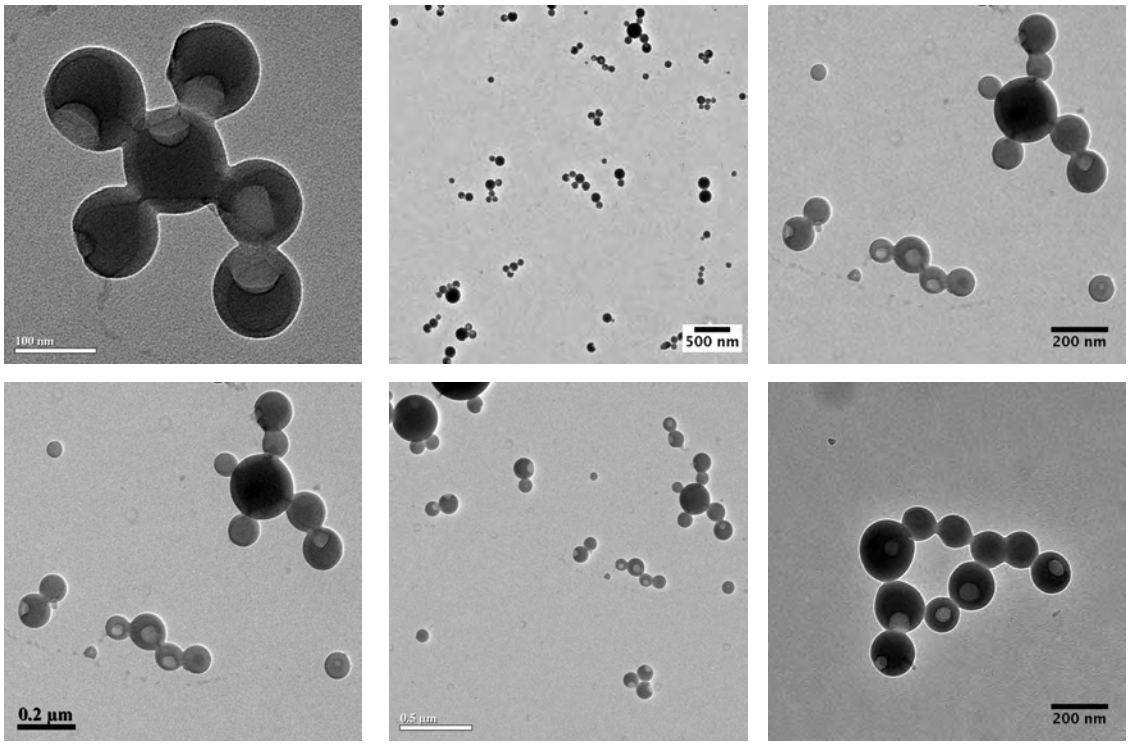

Figure S24: TEM images of **$(PS_{30})_2$-Zn** nanoparticles. Note the similar dimple size compared to **$(PS_{20})_4$-Zn** nanoparticles, which have comparable degrees of steric shielding around the porphyrin core.

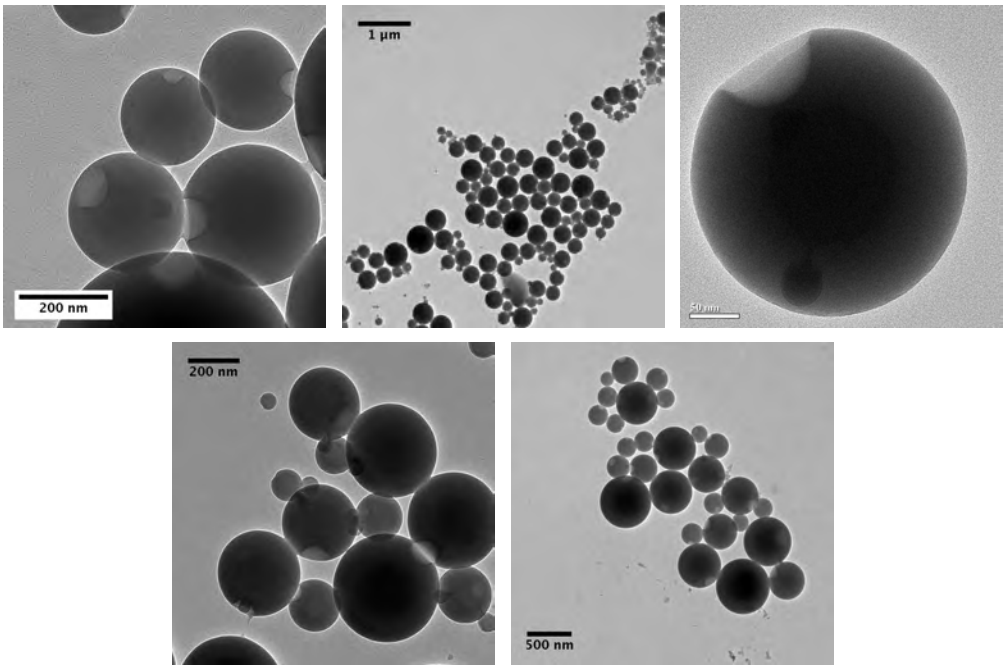

Figure S25: TEM images of $(\mathbf{PS}_{30})_2$**-H**$_2$ nanoparticles. The slightly smaller dimples compared to $(\mathbf{PS}_{30})_2$**-Zn** are consistent with weaker porphyrin–triazole interactions for the freebase porphyrin.

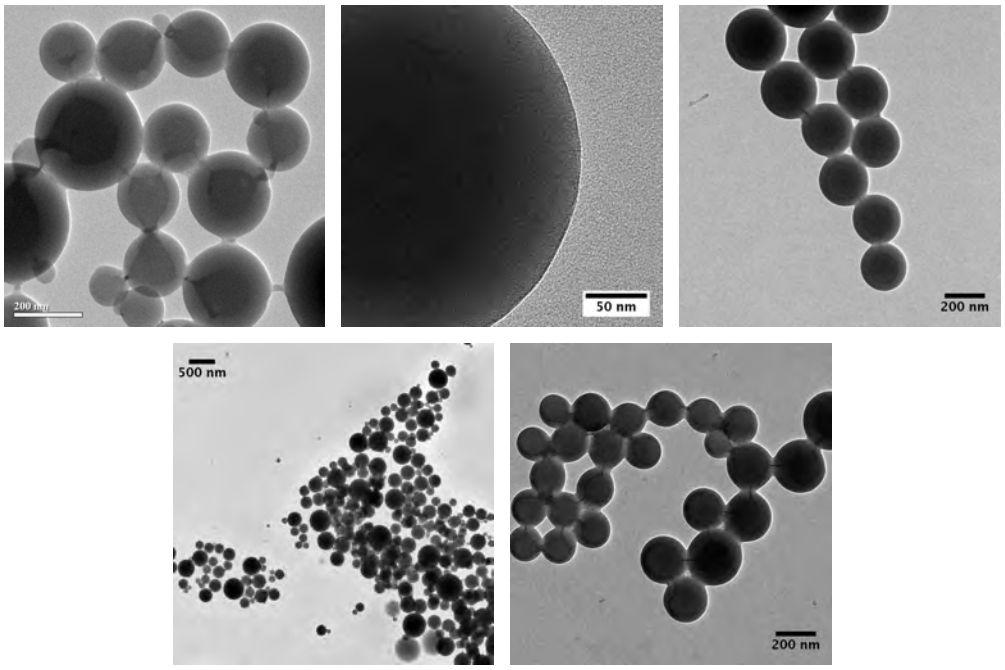

Figure S26: TEM images of $(\mathbf{PS}_{30})_4$**-Zn** nanoparticles. No dimples were observed on the surface of these nanoparticles, indicating that the particle viscosity was sufficiently low to completely expel any trapped solvent droplets before rigidifying.

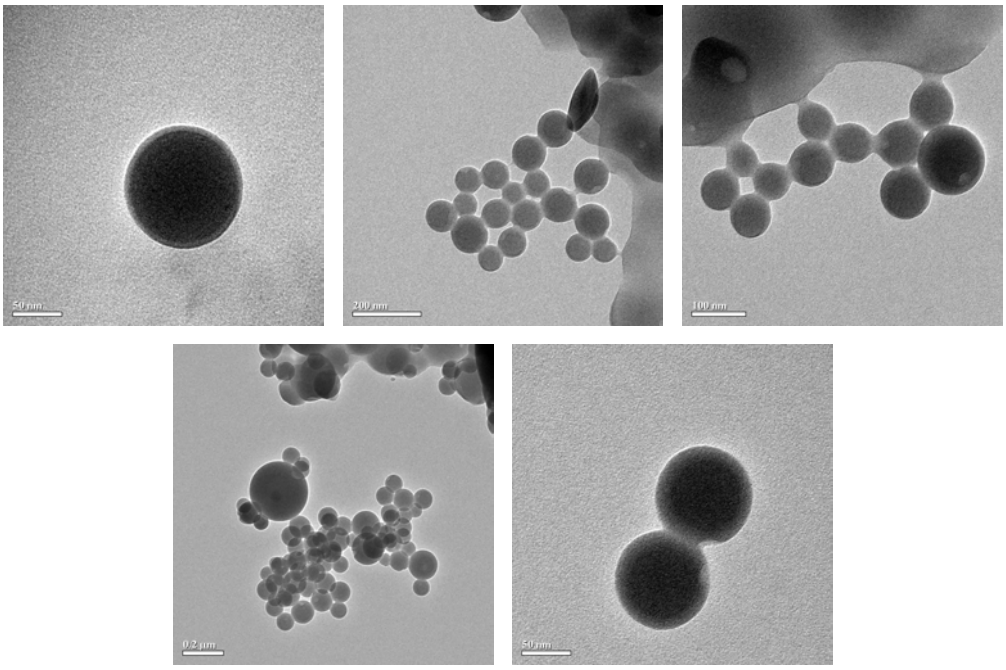

Figure S27: TEM images of $(\mathbf{PS}_{30})_4$-$\mathbf{H}_2$ nanoparticles.

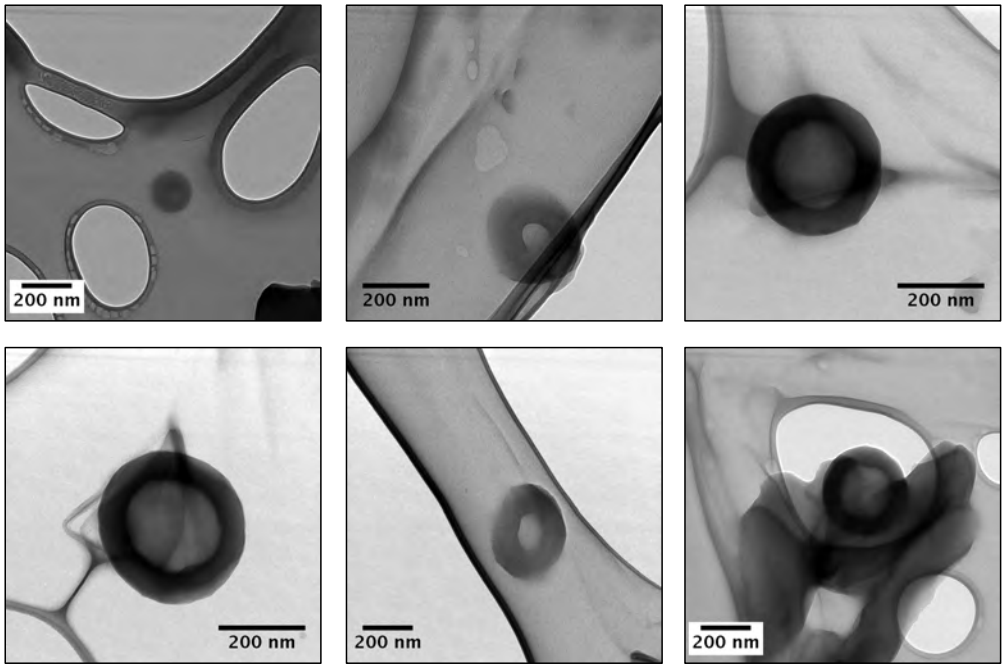

Figure S28: TEM images of cryo-microtomed nanoparticles, prepared from $(\mathbf{PS}_{20})_4$-**Zn**. These images verify that the particles do not have a vesicular bilayer boundary, and that the "dimples" penetrate into the body of the particles, as evidenced by the circular holes in their cross-sections.

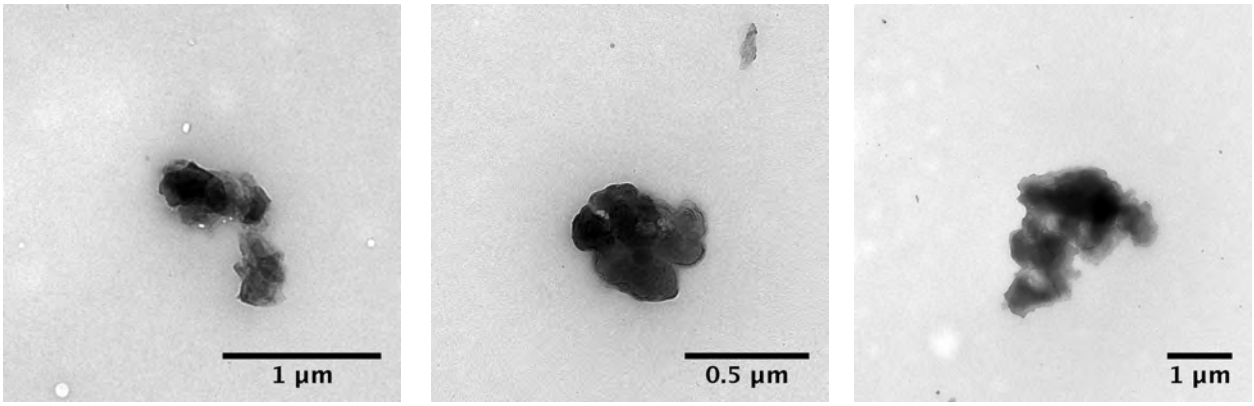

Figure S29: TEM images of **(PNIPAM$_{33}$)$_4$-Zn** aggregates.

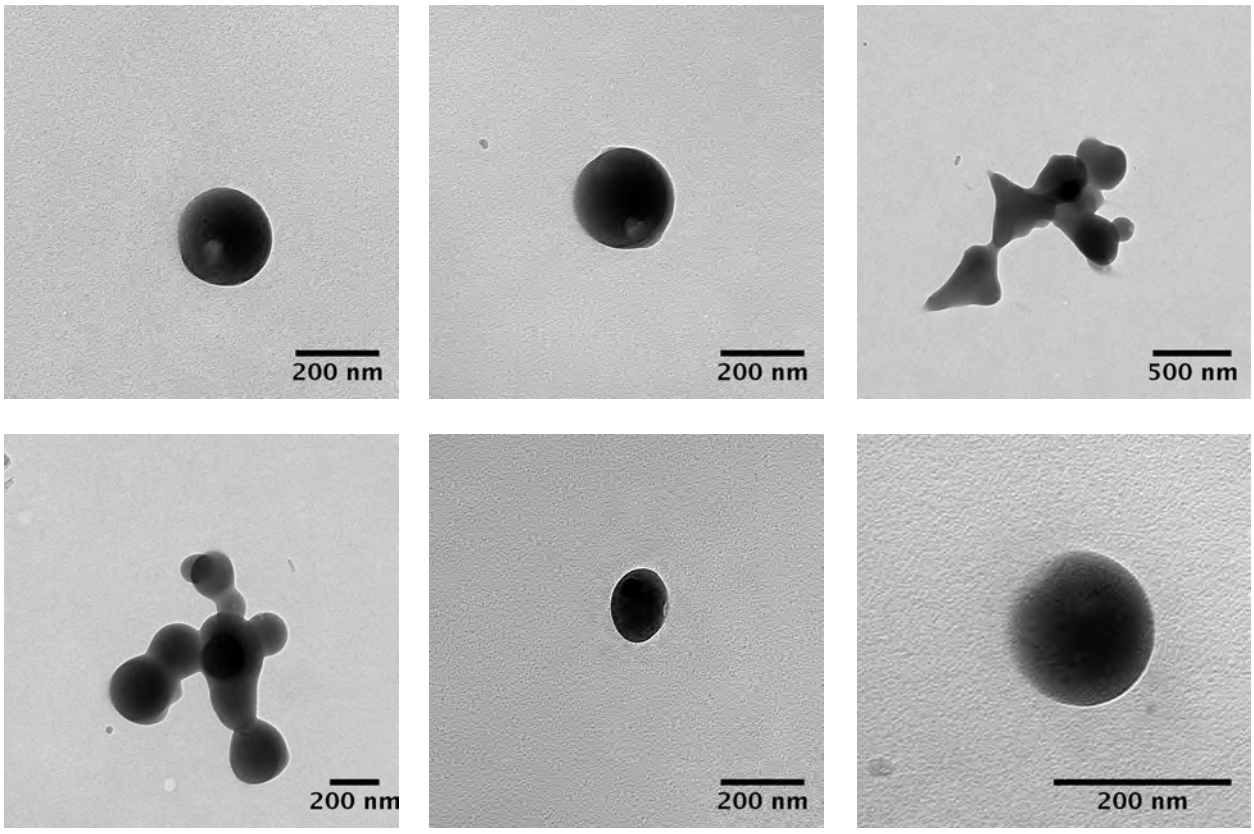

Figure S30: TEM images of **(PBA$_{15}$)$_4$-Zn** aggregates, formed under the same conditions used to prepare polystyrene-PPC nanoparticles. Particles show some rudimentary features in common with the dimpled polystyrene-PPC nanoparticles, but are not sufficiently rigid to maintain a robust and persistent morphology.

S.10 Fluorescence spectra and fluorescence micrographs of PPC nanoparticles

Solution-phase fluorescence spectra were recorded on a Cary Eclipse fluorescence spectrophotometer using 1×1 cm quartz fluorescence cuvettes. Fluorescence micrographs were recorded using a Olympus IX71 Total Internal Reflection Fluorescence (TIRF) inverted microscope operating in dark field mode. Fluorescence excitation was via a filtered xenon-mercury white light source. Micrographs were recorded digitally in black and white and false-coloured to the approximate fluorescence observed during the experiments.

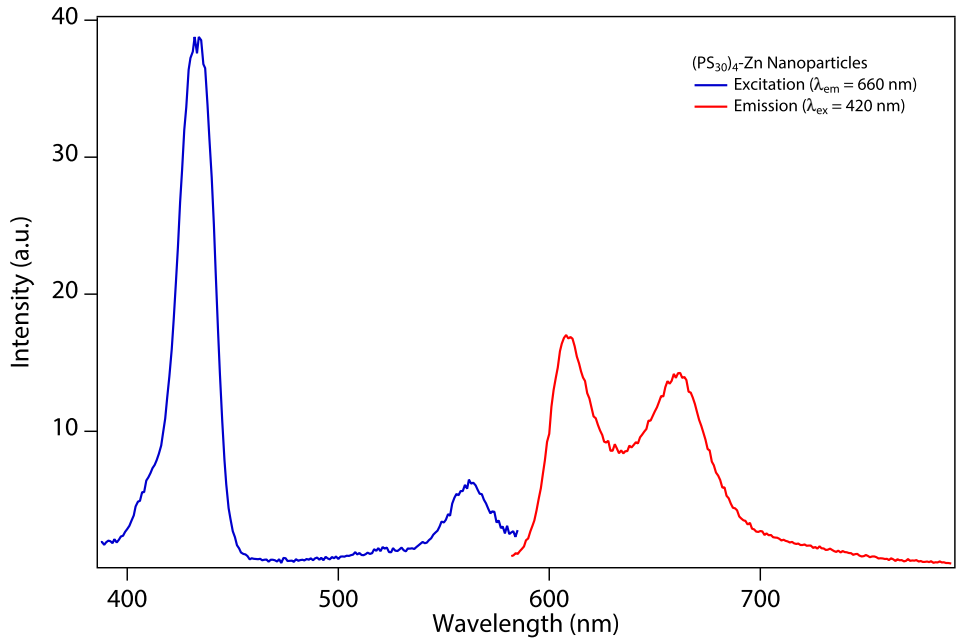

Figure S31: Fluorescence spectra of $(\mathbf{PS}_{30})_4$**-Zn** nanoparticle suspension in THF/water = 9:1 *v*/*v* (ca. 0.1 mg mL^{-1}).

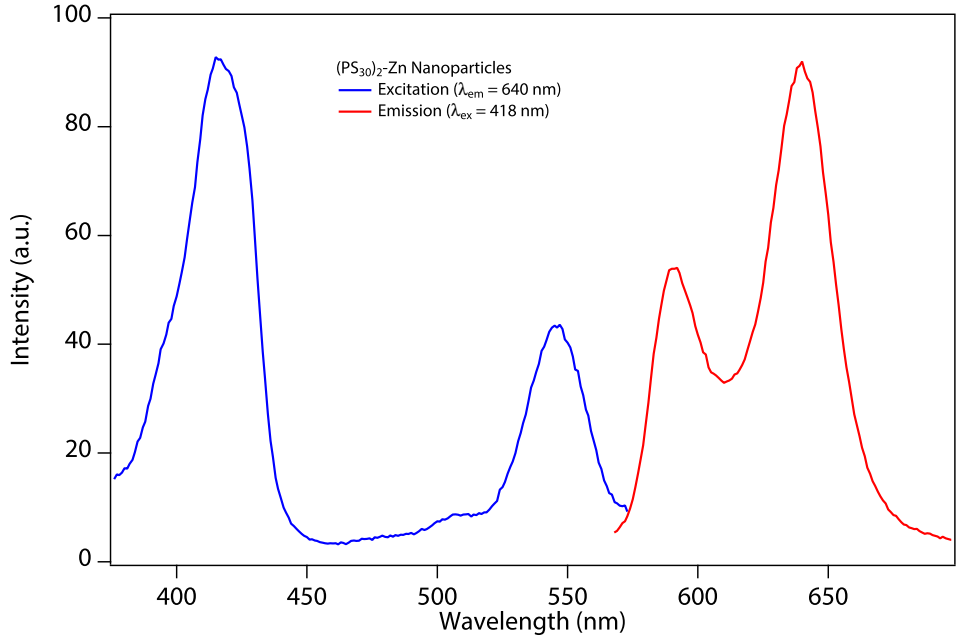

Figure S32: Fluorescence spectra of $(\mathbf{PS}_{30})_2$**-Zn** nanoparticle suspension in THF/water = 9:1 *v*/*v* (ca. 0.1 mg mL^{-1}).

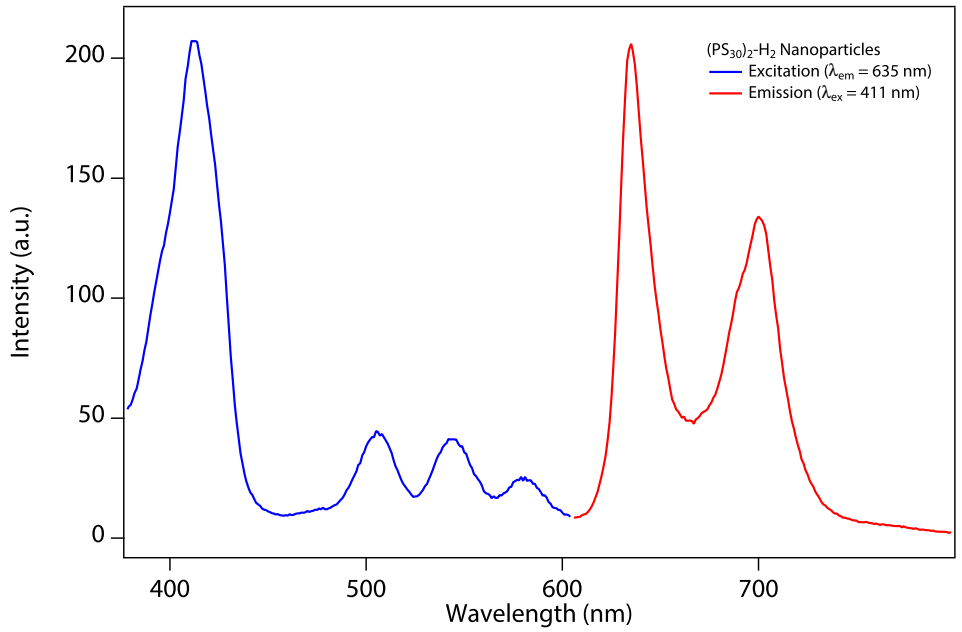

Figure S33: Fluorescence spectra of $(\mathbf{PS}_{30})_2$**-H**$_2$ nanoparticle suspension in THF/water = 9:1 *v*/*v* (ca. 0.1 mg mL^{-1}).

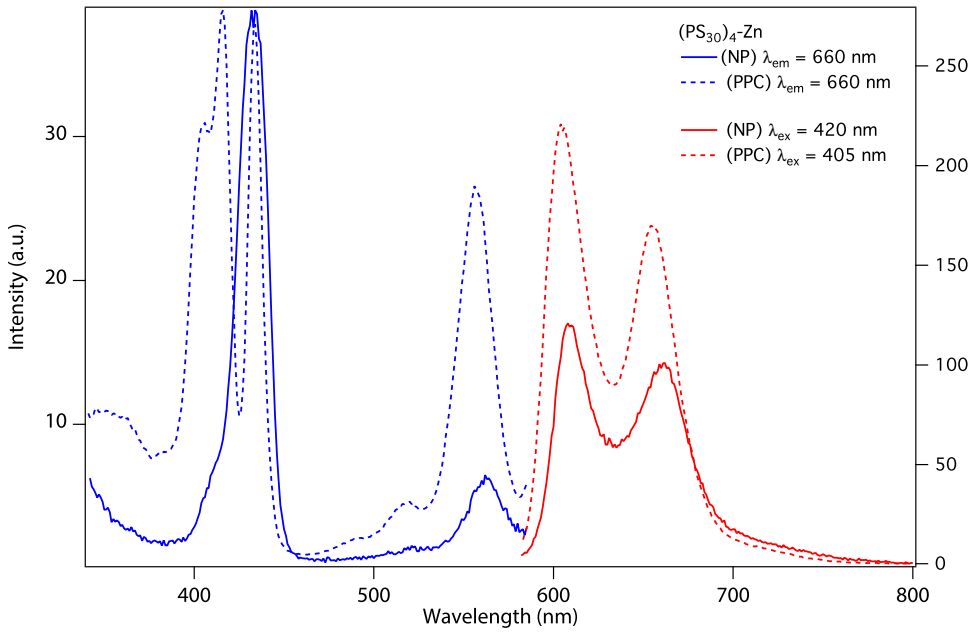

Figure S34: Comparison of fluorescence spectra of **(PS$_{30}$)$_4$-Zn** in THF (2 mM) (solid lines) and a suspension of **(PS$_{30}$)$_4$-Zn** (ca. 0.1 mg mL^{-1}).

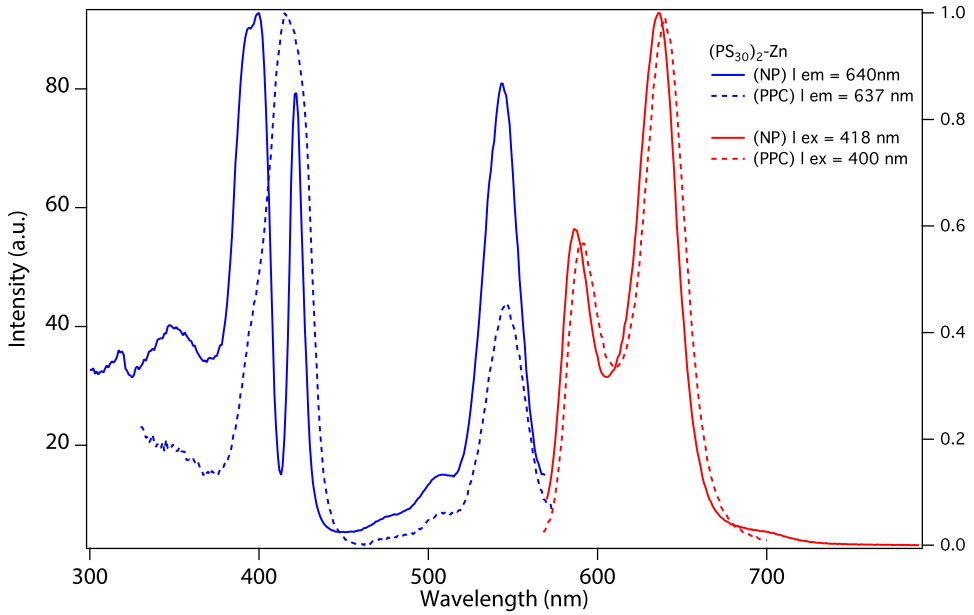

Figure S35: Comparison of fluorescence spectra of **(PS$_{30}$)$_2$-Zn** in THF (2 mM) (solid lines) and a suspension of **(PS$_{30}$)$_2$-Zn** (ca. 0.1 mg mL^{-1}).

S.11 Colourimetric acid sensing by freebase PPC nanoparticles

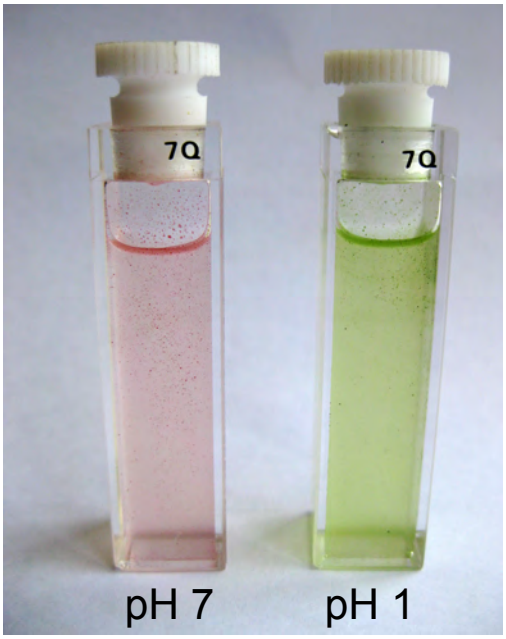

Figure S36: Colourimetric aqueous acid sensing by freebase PPC nanoparticles. Suspensions of **(PS$_{30}$)$_2$-Zn** nanoparticles suspensions in water (ca. 0.1 mg mL^{-1}) buffered to pH 7 and pH 1. The red and green colours of the suspensions are characteristic of freebase and protonated porphyrin macrocycles.

References

(1) Konkolewicz, D.; Gray-Weale, A.; Perrier, S. *J. Am. Chem. Soc.* **2009**, *131*, 18075–18077.

(2) Roberts, D. A.; Schmidt, T. W.; Crossley, M. J.; Perrier, S. *Chem.–Eur. J.* **2013**, *19*, 12759–12770.

(3) Armarego, W. L. F.; Chai, C. L. L. *Purification of Laboratory Chemicals*, 5th ed.; Butterworth-Heinemann: Burlington, MA, 2003.

(4) Chapman, R.; Jolliffe, K. A.; Perrier, S. *Aust. J. Chem.* **2010**, *63*, 1169–1172.

(5) Chapman, R.; Jolliffe, K. A.; Perrier, S. *Polym. Chem.* **2011**, *2*, 1956–1963.

(6) Blosi, M.; Albonetti, S.; Dondi, M.; Martelli, C.; Baldi, G. *J. Nanopart. Res.* **2011**, *13*, 127–138.

(7) Haitao, Z.; Canying, Z.; Yansheng, Y. *Nanotechnology* **2005**, *16*, 3079.

(8) Nakamura, T.; Tsukahara, Y.; Sakata, T.; Mori, H.; Kanbe, Y.; Bessho, H.; Wada, Y. *Bull. Chem. Soc. Jpn.* **2007**, *80*, 224–232.

(9) Yusa, S. I.; Endo, T.; Ito, M. *J. Polym. Sci., Part A: Polym. Chem.* **2009**, *47*, 6827–6838.

(10) Huisgen, R.; Szeimies, G.; Mobius, L. *Chem. Ber.* **1967**, *100*, 2494–2507.

(11) Huisgen, R. *1,3-Dipolar Cycloaddition Chemistry*; Wiley: New York, 1984.

(12) Arnold, D. P.; Blok, J. *Coord. Chem. Rev.* **2004**, *248*, 299–319.

(13) Arnold, D. P. *J. Chem. Educ.* **1988**, *65*, 1111–1112.

(14) Arnold, D. P. *Polyhedron* **1988**, *7*, 2225–2227.

(15) Kim, Y.; Mayer, M. F.; Zimmerman, S. C. *Angew. Chem., Int. Ed.* **2003**, *42*, 1121–1126.

(16) Brotherhood, P. R.; Luck, I. J.; Blake, I. M.; Jensen, P.; Turner, P.; Crossley, M. J. *Chem.–Eur. J.* **2008**, *14*, 10967–10977.

(17) Brotherhood, P. R.; Luck, I. J.; Crossley, M. J. *Magn. Reson. Chem.* **2009**, *47*, 257–262.

(18) Hawley, J. C.; Bampos, N.; Abraham, R. J.; Sanders, J. K. M. *Chem. Commun.* **1998**, 661–662.

(19) Kim, H. J.; Jo, H. J.; Kim, J.; Kim, S. Y.; Kim, D.; Kim, K. *CrystEngComm* **2005**, *7*, 417–420.

(20) Li, D.; Huang, K. K.; Hu, B.; Shi, Z.; Wang, G.; Feng, S. H. *J. Mol. Struct.* **2009**, *938*, 82–88.

(21) McMurtrie, J. C.; Arnold, D. P. *J. Struct. Chem.* **2010**, *51*, 107–113.

(22) Medforth, C. J.; Wang, Z. C.; Martin, K. E.; Song, Y. J.; Jacobsen, J. L.; Shelnutt, J. A. *Chem. Commun.* **2009**, 7261–7277.

(23) Rosengarten, B.; Bottcher, C.; Schulz, A.; Fuhrhop, J. H.; Siggel, U. *J. Porphyrins Phthalocyanines* **1998**, *2*, 273–284.

(24) Smith, G.; Arnold, D. P.; Kennard, C. H. L.; Mak, T. C. W. *Polyhedron* **1991**, *10*, 509–516.

(25) Webb, S. J.; Sanders, J. K. M. *Inorg. Chem.* **2000**, *39*, 5920–5929.

(26) Crossley, M. J.; Thordarson, P.; Wu, R. A. S. *J. Chem. Soc. Perkin Trans. 1* **2001**, 2294–2302.

(27) Rothemund, P.; Menotti, A. R. *J. Am. Chem. Soc.* **1948**, *70*, 1808–1812.

(28) Aminabhavi, T. M.; Gopalakrishna, B. *J. Chem. Eng. Data* **1995**, *40*, 856–861.